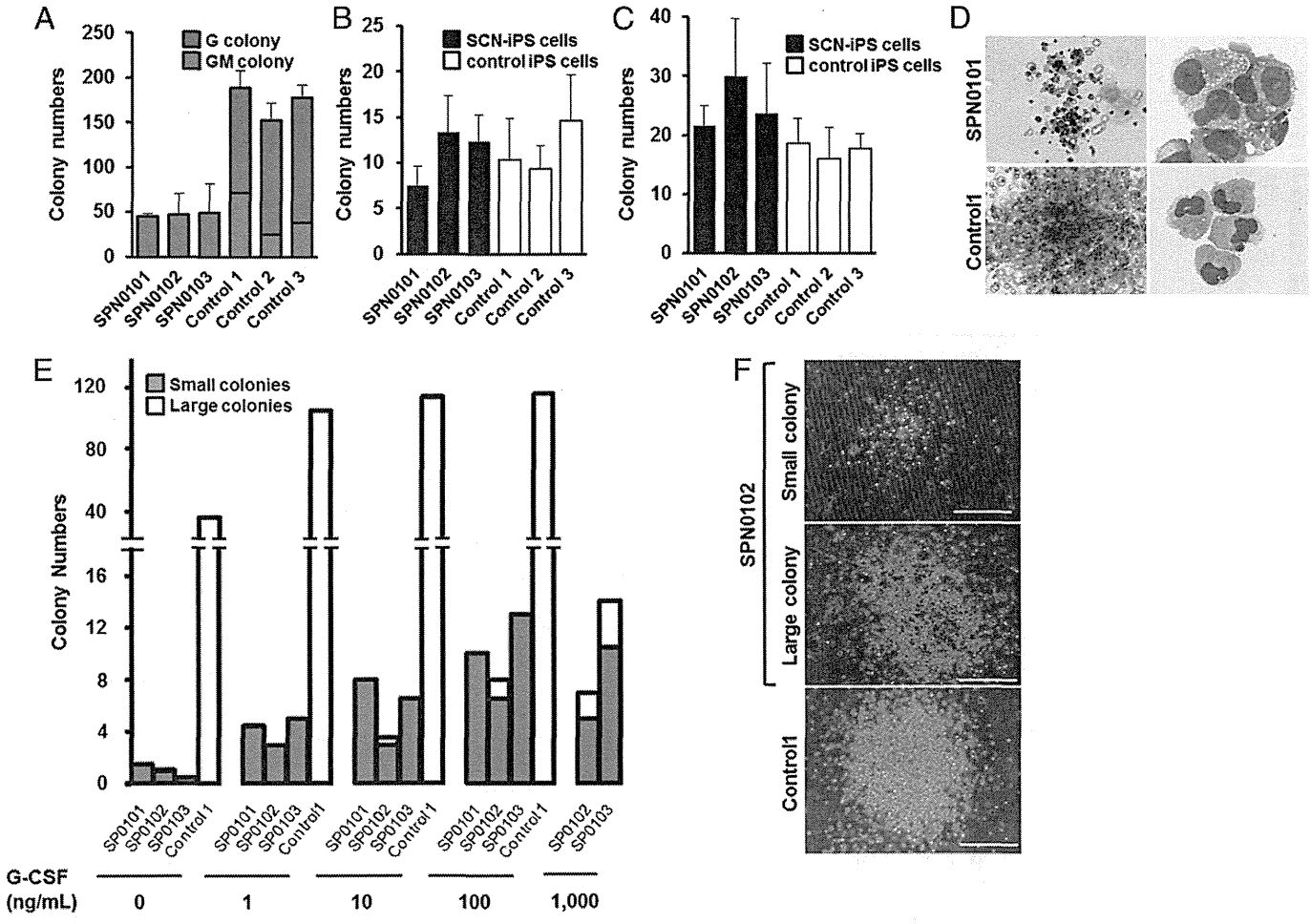

Fig. 1. Impaired neutrophil development from SCN-iPS cells. (*A*–C) A hematopoietic colony assay was performed by using 1×10^4 CD34$^+$ cells derived from three SCN-iPS cell clones (SPN0101, SPN0102, and SPN0103) and three control iPS cell clones (controls 1, 2, and 3) in the presence of a cytokine mixture. Colonies were sorted as myeloid (*A*), erythroid (*B*), and mixed-lineage (Mix) (*C*). Data are shown as mean ± SD. (*D*) Photographs of colonies (*Left*; 100×) and cells in a GM colony (*Right*; 400×; May–Grünwald–Giemsa staining). (*E*) A hematopoietic colony assay with dose escalation of G-CSF was performed by using 1×10^5 CD34$^+$ cells derived from SCN-iPS and control iPS cells. Filled and open bars indicate small colonies consisting of <100 cells and large colonies consisting of >100 cells, respectively. Data are shown as the average of three independent experiments. (*F*) Photographs of a small colony derived from SCN-iPS cells (SPN0102) in the presence of 10 ng/mL G-CSF, large colonies derived from SCN-iPS cells in the presence of 1,000 ng/mL G-CSF, and large colonies derived from control iPS cells (control 1) in the presence of 10 ng/mL G-CSF. (Scale bars, 200 μm.)

and *D*). In particular, only a few SCN-iPS cell-derived granulocyte (G) colonies—myeloid colonies consisting of only granulocytes—were detected (Fig. 1*A*). SCN-iPS cell-derived granulocyte–macrophage (GM) colonies—myeloid colonies consisting of macrophages/monocytes with/without granulocytes—contained a few immature myeloid cells in addition to macrophages/monocytes, whereas control iPS cell-derived GM colonies included a substantial number of mature, segmented, and band neutrophils (Fig. 1*D*).

We also found that Mix colonies derived from SCN-iPS cells, but not control iPS cells, contained immature myeloid cells and few mature neutrophils (Fig. S2 *C* and *D*). Next, we conducted a hematopoietic colony assay using various concentrations of G-CSF alone instead of the cytokine mixture to examine the G-CSF dose dependency of neutrophil differentiation from SCN-iPS and control iPS–CD34$^+$ cells. For all concentrations of G-CSF used (1–1,000 ng/mL), the SCN-iPS cell-derived myeloid colonies were significantly lower in number and smaller in size than the control iPS cell-derived myeloid colonies (Fig. 1*E*). Myeloid colony formation from control iPS cells reached a plateau at ~1–10 ng/mL G-CSF, whereas the number and size of those from SCN-iPS cells gradually increased with increasing concentrations of G-CSF. However, the values observed for SCN-iPS cells did not reach those for the control iPS cells, even at the highest dose of G-CSF used (1,000 ng/mL). Furthermore, large colonies consisting of >100 cells derived from SCN-iPS cells were only found with higher concentrations of G-CSF (Fig. 1*F*). Thus, granulopoiesis initiated from SCN-iPS cells was relatively insensitive to G-CSF, reflecting the inadequate in vivo response of neutrophils to G-CSF in SCN patients (14, 15). Therefore, these results support the applicability of the SCN-iPS cells established herein as a disease model for SCN.

To examine neutrophil development from SCN-iPS cells in more detail, SCN-iPS and control iPS–CD34$^+$ cells (1×10^4 cells each) were cocultured in suspension with AGM-S3 cells in the presence of neutrophil differentiation medium (*SI Materials and Methods*). The number of nonadherent cells derived from SCN-iPS–CD34$^+$ cells was lower than that from control iPS–CD34$^+$ cells on day 14 of culture (SCN-iPS cells, $9.77 \times 10^4 \pm 1.65 \times 10^4$ cells; control iPS cells, $52.48 \times 10^4 \pm 23.13 \times 10^4$ cells; $P < 0.05$) (Fig. 2*A*). The proportion of mature neutrophils among the nonadherent cells was also significantly lower for SCN-iPS cells relative to control iPS cells on day 14 (SPN-iPS cells, 15.53% ± 4.33%; control iPS cells, 71.285 ± 3.30%; $P < 0.05$) (Fig. 2 *B* and *C*), indicating that myeloid cells derived from SCN-iPS cells revealed the maturation arrest in the neutrophil development. We then examined a possibility that the maturation arrest in SCN-

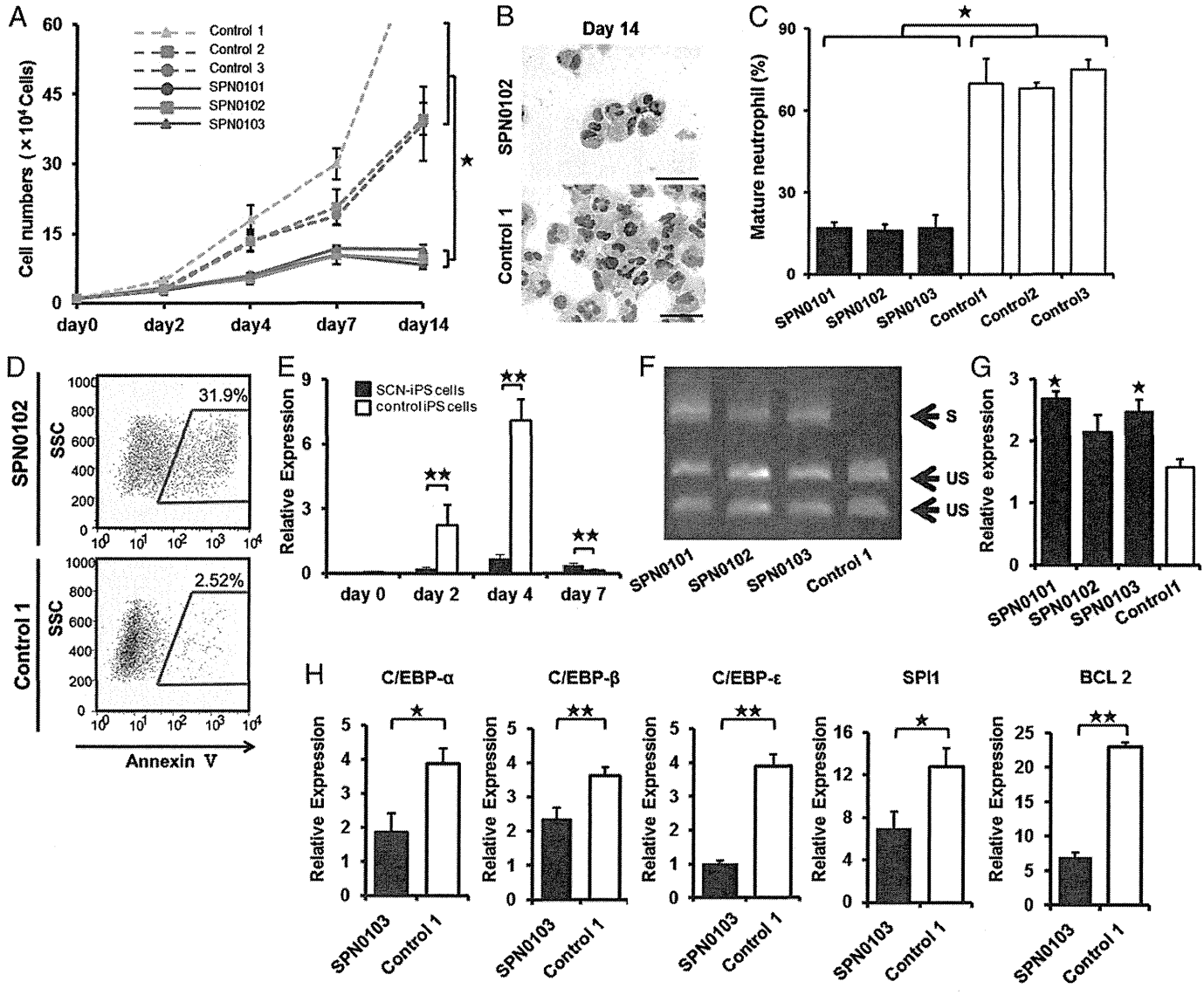

Fig. 2. Analysis of impaired neutrophil development from SCN-iPS cells. (*A*) Total number of nonadherent cells in the suspension culture of 1×10^4 $CD34^+$ cells derived from SCN-iPS and control iPS cells. Data are shown as mean ± SD. $^*P < 0.01$. (*B*) Photographs of nonadherent cells derived from SCN-iPS (SPN0103) and control iPS cells (control 1) on day 14 of culture (400×; May–Grünwald–Giemsa staining; scale bars, 50 μm.) (*C*) Filled and open bars show the proportion of mature neutrophils among the cells derived from SCN-iPS (filled bars) and control iPS (open bars) cells on day 14 of suspension culture. Data are shown as mean ± SD. $^*P < 0.05$. (*D*) Flow cytometric analysis of annexin V expression on cultured cells from SCN-iPS cells (SPN0102) or control iPS cells (control 1) on day 7. (*E*) Sequential qRT-PCR analysis of the relative expression of ELANE mRNA [ELANE/hypoxanthine–guanine phosphoribosyltransferase (HPRT) expression]. Data obtained from independent experiments using three SCN-iPS cell clones (SPN0101, SPN0102, and SPN0103) and three control iPS cell clones are shown as mean ± SD. $^{**}P < 0.01$. (*F* and *G*) $CD34^+$ cells derived from SCN-iPS or control iPS cells were cultured in neutrophil differentiation medium (see text). On day 7, nonadherent cells were collected and analyzed. (*F*) Representative gel showing spliced (S) and unspliced (US) XBP-1 bands on day 7. (*G*) qRT-PCR analysis of the relative mRNA expression (target/HPRT expression) of BiP on day 7. Data are shown as mean ± SD. $^*P < 0.05$; different from control 1). (*H*) qRT-PCR analysis of the relative mRNA expression (target / HPRT expression) of C/EBP-α, C/EBP-β, C/EBP-ε, SPI1, and BCL2 genes in non-adherent cells derived from SCN-iPS cells (filled bars, SPN0103) and control iPS cells (open bars, control 1) on day 2 of suspension culture. Data are shown as the mean ± the s.d. ($^{**}P < 0.01$, $^*P < 0.05$).

iPS cell-derived myeloid cells might be caused by their apoptosis. In flow cytometric analysis, SCN-iPS cell-derived myeloid cells contained a significantly higher proportion of annexin V-positive cells than control iPS-derived myeloid cells on day 7 of culture, suggesting that the maturation arrest in myeloid cells derived from SCN-iPS cells might be caused by their apoptosis (Fig. 2*D*).

We next examined ELANE mRNA expression levels in nonadherent cells derived from SCN-iPS vs. control iPS cells (Fig. 2*E*). ELANE expression was significantly lower in nonadherent cells derived from SCN-iPS vs. control iPS cells on days 2 and 4 of culture ($P < 0.01$), as reported (16, 17). However, the former was a little higher than the latter on day 7 ($P < 0.01$). This result may be explained by the existence of SCN-iPS cell-derived myeloid cells arrested at an early stage along the neutrophil differentiation pathway even on day 7 of culture. We also examined the expression of proteinase 3 and azurocidin, which comprise a family of closely related genes encoding neutrophil granule proteins along with ELANE, and found these genes were more highly expressed on day 4 (Fig. S3).

It has been reported that induction of the endoplasmic reticulum stress (ER) response and the unfolded protein response (UPR) has been advanced as a potential explanation for the molecular pathogenesis of SCN (18, 19). Thus, we examined activation of the UPR by X-box binding protein 1 (XBP-1) mRNA splicing on day 7. As shown in Fig. 2*F*, SPN-iPS cells induced XBP-1 mRNA splicing. We also found the up-regulation of BiP

(also known as GRP78 or HSPA5) (Fig. 2*G*). These results suggested that ER stress response and UPR might be involved in the pathogenesis in SCN.

To examine further the differences in gene expression between the two cell types, a microarray analysis was carried out by using $CD34^+$ cells derived from SCN-iPS and control iPS cells (three clones of each) in suspension culture on day 2. At this early time point, differences in cell number and morphology were not yet readily discernible between SCN-iPS and control iPS cells, as shown in Fig. 2*A*. However, the microarray analysis revealed a differential expression of various genes between the two cell types. Transcription factor genes, which were related to neutrophil development [e.g., CCAAT/enhancer-binding protein (C/EBP)-α (20), C/EBP-β (21), C/EBP-ε (22), and SPI1 (also known as PU.1) (23)], were all down-regulated in SCN-iPS cells. B-cell chronic lymphocytic leukemia/lymphoma 2, which regulates cell death under ER stress through the core mitochondrial apoptosis pathway (24), was also down-regulated (Fig. 3*A*). These findings were confirmed by quantitative reverse-transcriptional PCR (qRT-PCR), as shown in Fig. 2*H*.

Notably, the down-regulation of the genes in SCN-iPS cells related to and regulated by the wingless-type mmtv integration site family, member 3a (Wnt3a)/β-catenin pathway [e.g., Wnt3a, lymphoid enhance-binding factor (LEF)-1, BIRC5 (also known as survivin), and cyclin D1] was also uncovered by microarray analysis and qRT-PCR (Fig. 3 *A–C* and Fig. S4). Therefore, we examined the effect of enhancement of Wnt3a/β-catenin signaling by exogenous Wnt3a addition on the neutrophil development of $CD34^+$ cells derived from SCN-iPS and control iPS cells. Although Wnt3a did not stimulate the survival, proliferation, and differentiation of $CD34^+$ cells derived from both iPS cells in the absence of cytokines stimulating myelopoiesis including G-CSF, the addition of Wnt3a to the neutrophil differentiation medium induced a dose-dependent increase in the percentage of mature neutrophils among the cultured cells, as shown in Fig. 3 *D* and *E*. Furthermore, when Wnt3a was added concurrently with 1,000ng/mL G-CSF, the proportion of mature neutrophils increased more than it did with Wnt3a or 1,000 ng/mL G-CSF alone, reaching a value comparable with that observed for control iPS cells (Fig. 4 *A* and *B*).

The reduced expression of LEF-1 (as regulated by the Wnt3a/β-catenin pathway) reportedly plays a critical role in the defective maturation of neutrophils in SCN patients (25). Therefore, we next examined LEF-1 mRNA expression in SCN-iPS–$CD34^+$ cells cultured in the presence of Wnt3a, G-CSF (1,000 ng/mL), or both. Wnt3a and G-CSF both enhanced LEF-1 mRNA expression, but the most significant increase was observed in the presence of Wnt3a plus G-CSF. LEF-1 expression in SCN-iPS–$CD34^+$ cells in response to Wnt3a plus G-CSF was almost the same as that in control iPS–$CD34^+$ cells (Fig. 4*C*). These results substantiate the importance of LEF-1 in neutrophil development and the pathogenesis of SCN, as shown (25). Moreover the

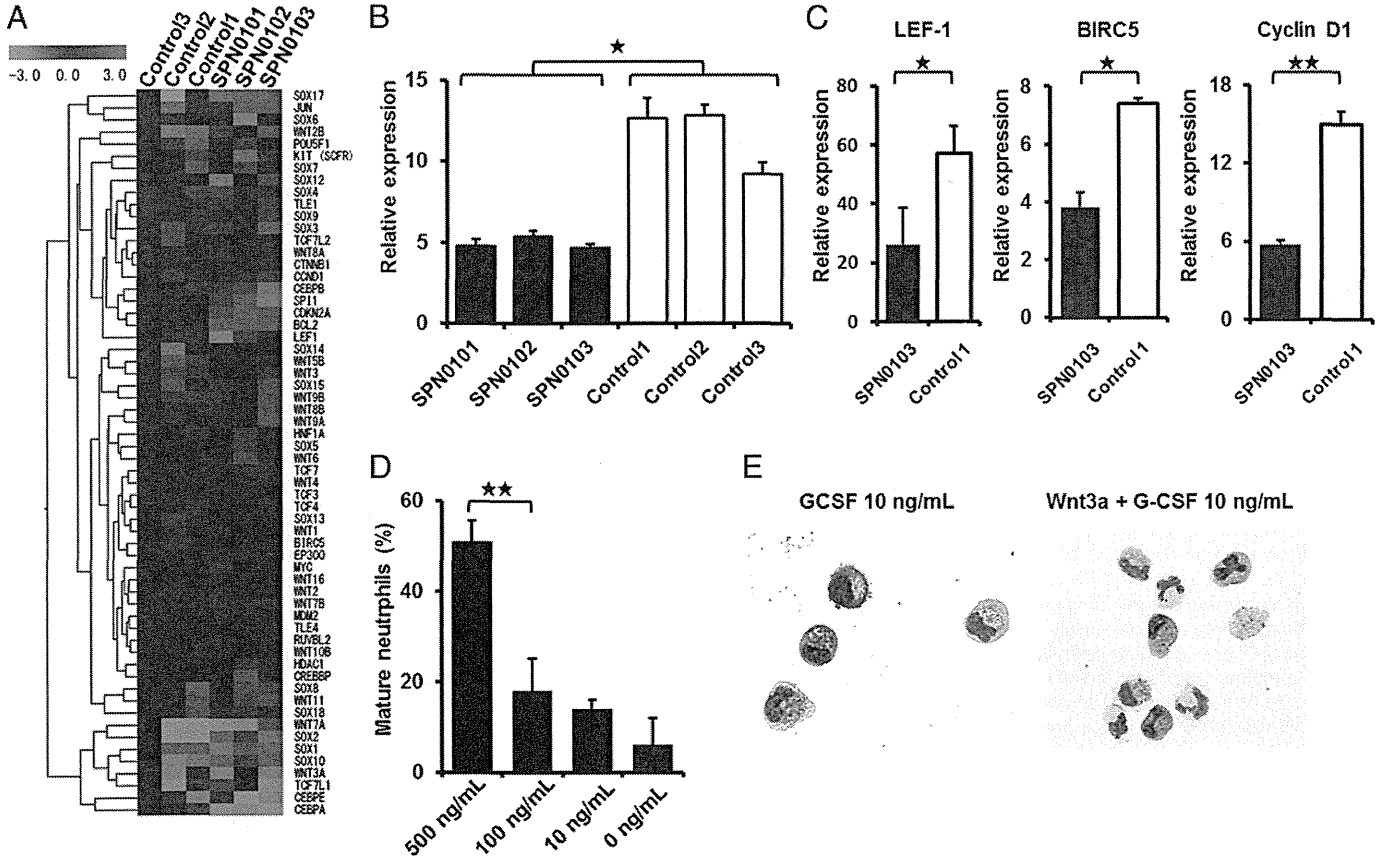

Fig. 3. Effects of Wnt3a on neutrophil development from SCN-iPS cells. (*A*) Heat map showing differential gene expression among SCN-iPS and control iPS cells on day 2. Red, high gene expression; blue, low gene expression compared with gene expression in control 3. (*B*) qRT-PCR analysis of the relative mRNA expression (target/HPRT expression) of Wnt3a on day 2. Filled and open bars indicate experiments using SCN-iPS cells (SPN0101, SPN0102, and SPN0103) and control iPS cells (controls 1, 2, and 3), respectively. Data are shown as mean ± SD. $^*P < 0.05$. (*C*) qRT-PCR analysis of the relative expression (target/HPRT expression) of genes regulated by the Wnt3a/β-catenin pathway (LEF-1, survivin, and cyclin D1) in SCN-iPS cells (filled bars, SPN0103) vs. control iPS cells (open bars, control 1) on day 2 of suspension culture. Data are shown as mean ± SD. $^{**}P < 0.01$; $^*P < 0.05$. (*D*) Proportion of mature neutrophils among the cells derived from SCN-iPS cells (SPN0102) on day 14 of suspension culture with dose escalation of Wnt3a. Data are shown as mean ± SD. $^{**}P < 0.01$. (*E*) Photographs of nonadherent cells on day 7 of suspension culture with or without Wnt3a (500 ng/mL) (400×; May–Grünwald–Giemsa staining).

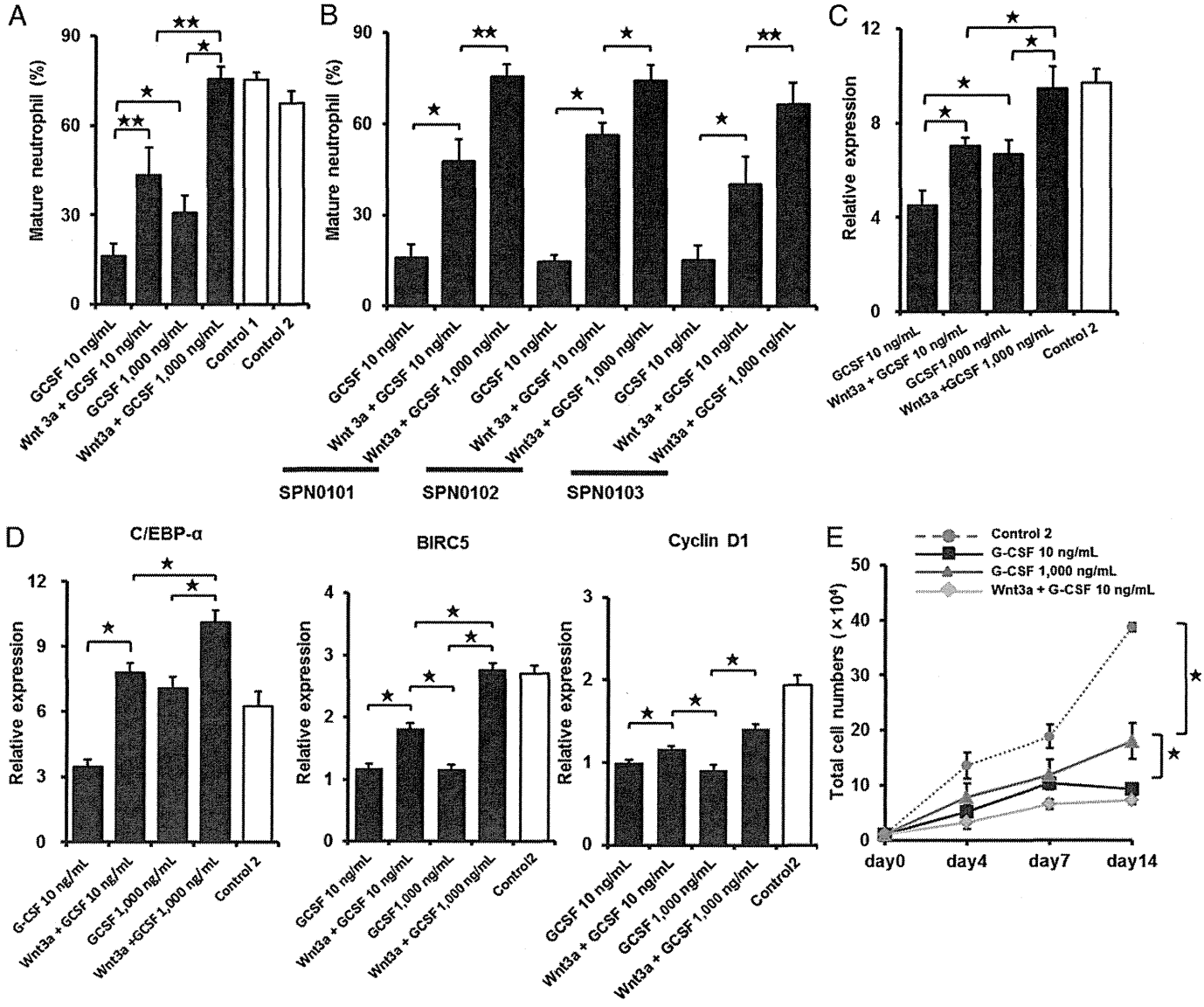

Fig. 4. Effects of Wnt3a in combination with high-dose G-CSF. (*A*) Filled and open bars show the proportion of mature neutrophils among the cells derived from SCN-iPS cells (SPN0101) on day 14 of suspension culture in the presence of neutrophil differentiation medium containing 10 ng/mL G-CSF (GCSF 10 ng/mL); 500 ng/mL Wnt3a and 10 ng/mL G-CSF (Wnt3a+GCSF 10 ng/mL); 1,000 ng/mL G-CSF (GCSF 1,000 ng/mL); or 500 ng/mL Wnt3a and 1,000 ng/mL G-CSF (Wnt3a + GCSF 1,000 ng/mL); and that from control iPS cells (controls 1 and 2) cultured in the neutrophil differentiation medium containing 10 ng/mL G-CSF, respectively. Data are shown as mean ± SD. $^{**}P < 0.01$; $^{*}P < 0.05$. (*B*) The proportion of mature neutrophils among the cells derived from three SCN-iPS cell clones (SPN0101, SPN0102, and SPN0103) on day 14 of suspension culture in the presence of neutrophil differentiation medium containing 10 ng/mL G-CSF (GCSF 10 ng/mL); 500 ng/mL Wnt3a and 10 ng/mL G-CSF (Wnt3a+GCSF 10 ng/mL); or 500 ng/mL Wnt3a and 1,000 ng/mL G-CSF (Wnt3a + GCSF 1,000 ng/mL). Data are shown as mean ± SD. $^{**}P < 0.01$; $^{*}P < 0.05$. (*C*) Filled and open bars show the relative expression (target/HPRT expression) of LEF-1 mRNA in SCN-iPS cells (SPN0101) on day 2 of suspension culture in the presence of differentiation medium containing the same combinations of Wnt3a and G-CSF as shown in *A* and that from control iPS cells (control 2), respectively. Data are shown as mean ± SD. $^{**}P < 0.01$; $^{*}P < 0.05$. (*D*) Filled and open bars show the relative expression (target/HPRT expression) of C/EBP-α, BIRC5, or cyclin D1 mRNA in SCN-iPS cells (SPN0101) on day 2 of suspension culture in the presence of differentiation medium containing the same combinations of Wnt3a and G-CSF as shown in *A* and that from control iPS cells (control 2), respectively. Data are shown as mean ± SD. $^{**}P < 0.01$; $^{*}P < 0.05$. (*E*) Total cell numbers of nonadherent cells in suspension cultures of 1×10^4 $CD34^+$ cells derived from control iPS cells (control 2; red broken line) and SCN-iPS cells (SPN0101) in the presence of neutrophil differentiation medium (black line) and those from SCN-iPS cells in the presence of neutrophil differentiation medium containing 500 ng/mL Wnt3a (yellow line) or 1,000 ng/mL G-CSF (black line). Data are shown as mean ± SD. $^{**}P < 0.05$.

administration of Wnt3a led to up-regulate C/EBP-α, cyclin D1, and BIRC5/survivin in addition to LEF-1 in the presence of G-CSF (Fig. 4*D*). These results suggested that the up-regulation of LEF-1 expression might promote granulopoiesis by increasing the expressions of cyclin D1, BIRC5/survivin, and C/EBP-α and its binding to LEF-1 in accordance with the previous report (25). Interestingly, Wnt3a did not stimulate the proliferation of myeloid cells, whereas 1,000 ng/mL G-CSF did to a certain extent (Fig. 4*E*). Hence, Wnt3a was capable of stimulating the maturation of impaired neutrophils in the presence of G-CSF, but not the proliferation of myeloid cells from SCN-iPS cells.

Importantly, aside from providing new insights into the mechanisms behind impaired neutrophil development in SCN patients, the present study demonstrates that agents activating the Wnt3a/β-catenin pathway are potential candidates for new drugs for SCN with mutations in the ELANE gene. Because endogenous G-CSF is readily increased in SCN patients (26), these activating agents may be viable alternatives to exogenous G-CSF treatment.

Materials and Methods

Additional information is available in *SI Materials and Methods*.

Generation of Human iPS Cells. BM fibroblasts from a patient with SCN and skin dermal fibroblasts from a healthy donor were acquired after obtaining informed consent after getting the approval by the Ethics Committee of the Institute of Medical Science, University of Tokyo, in accordance with the Declaration of Helsinki. The SCN patient presented with a heterozygous mutation in the ELANE gene in the 707 region of exon 5. SCN-iPS cells were established from the SCN-BM fibroblasts by transfection with the pMX retroviral vector, as described (10). This vector expressed the human transcription factors OCT3/4, SOX2, KLF4, and c-MYC. Control iPS cell clones, control 1 (TkDN4-M) and control 3 (201B7), were gifts from K. Eto and S. Yamanaka (Kyoto University, Kyoto), respectively (10, 11). Control 2 (SPH0101) was newly generated from another healthy donor's skin dermal fibroblasts by using the same methods.

Hematopoietic Colony Assay. A hematopoietic colony assay was performed in an aliquot of culture mixture, which contained 1.2% methylcellulose (Shin-Etsu Chemical), 30% (vol/vol) FBS, 1% (vol/vol) deionized fraction V BSA, 0.1 mM 2-mercaptoethanol (2-ME), α-minimum essential medium, and a cytokine mixture consisting of 100 ng/mL human stem cell factor (hSCF) (Wako), 100 ng/mL fusion protein 6 [FP6; a fusion protein of interleukin (IL)-6 and IL-6 receptor] (a gift from Tosoh), 10 ng/mL human IL-3 (hIL-3) (a gift from Kirin Brewery), 10 ng/mL human thrombopoietin (hTPO) (a gift from Kirin Brewery), 10 ng/mL human G-CSF (a gift from Chugai Pharmaceutical), and 5 U/mL human erythropoietin (a gift from Kirin Brewery). For dose escalation experiments, various concentrations (0, 1, 10, 100, and 1,000 ng/mL) of G-CSF were used instead of the cytokine mixture described above. Colony types were determined according to established criteria on day 14 of culture by in situ observations under an inverted microscope (IX70; Olympus) (27).

Suspension Culture and Neutrophil Differentiation Assay. $CD34^+$ cells (1×10^4 cells) were cocultured with irradiate confluent AGM-S3 cells in neutrophil differentiation medium containing Iscove's modified Dulbecco's medium, 10% FBS, 3 mM L-glutamine, 1×10^{-4} M 2-ME, 1×10^{-4} M nonessential amino acids solution, 100 ng/mL hSCF, 100 ng/mL FP6, 10 ng/mL hIL-3, 10 ng/mL hTPO, and 10 or 1,000 ng/mL human G-CSF. Wnt3a (10, 100, or 500 ng/mL) (R&D) was then added. The medium was replaced with an equivalent volume of fresh medium every 4 d. Living, nonadherent cells were counted following 0.4% trypan blue staining.

PCR primer. All primer sets used in this study are shown in Table S1.

Statistical Analysis. All data are presented as mean ± SD. $P < 0.05$ was considered significant. Statistical analyses were performed by using Prism software (GraphPad).

ACKNOWLEDGMENTS. We thank the individual with SCN who participated in this study; K. Eto for providing control iPS cells (control 1; TkDN4-M); S. Yamanaka for providing control iPS cells (control 3; 206B7); and E. Matsuzaka and S. Hanada for technical assistance. This work was supported by in part by Ministry of Education, Culture, Sports, Science, and Technology of Japan (MEXT) Grants-in-Aid (to Y.E.) and Project for Realization of Regenerative Medicine (MEXT) Grants-in-Aid (to K.Tsuji).

1. Zeidler C, Germeshausen M, Klein C, Welte K (2009) Clinical implications of *ELA2-, HAX1-*, and G-CSF-receptor (*CSF3R*) mutations in severe congenital neutropenia. *Br J Haematol* 144(4):459–467.
2. Freedman MH, et al. (2000) Myelodysplasia syndrome and acute myeloid leukemia in patients with congenital neutropenia receiving G-CSF therapy. *Blood* 96(2):429–436.
3. Dale DC, et al. (1993) A randomized controlled phase III trial of recombinant human granulocyte colony-stimulating factor (filgrastim) for treatment of severe chronic neutropenia. *Blood* 81(10):2496–2502.
4. Rosenberg PS, et al.; Severe Chronic Neutropenia International Registry (2006) The incidence of leukemia and mortality from sepsis in patients with severe congenital neutropenia receiving long-term G-CSF therapy. *Blood* 107(12):4628–4635.
5. Xia J, et al. (2009) Prevalence of mutations in ELANE, GFI1, HAX1, SBDS, WAS and G6PC3 in patients with severe congenital neutropenia. *Br J Haematol* 147(4):535–542.
6. Horwitz MS, et al. (2007) Neutrophil elastase in cyclic and severe congenital neutropenia. *Blood* 109(5):1817–1824.
7. Hajjar E, Broemstrup T, Kantari C, Witko-Sarsat V, Reuter N (2010) Structures of human proteinase 3 and neutrophil elastase—so similar yet so different. *FEBS J* 277(10): 2238–2254.
8. Fouret P, et al. (1989) Expression of the neutrophil elastase gene during human bone marrow cell differentiation. *J Exp Med* 169(3):833–845.
9. Pham CT (2006) Neutrophil serine proteases: Specific regulators of inflammation. *Nat Rev Immunol* 6(7):541–550.
10. Takayama N, et al. (2010) Transient activation of c-MYC expression is critical for efficient platelet generation from human induced pluripotent stem cells. *J Exp Med* 207(13):2817–2830.
11. Takahashi K, et al. (2007) Induction of pluripotent stem cells from adult human fibroblasts by defined factors. *Cell* 131(5):861–872.
12. Germeshausen M, Ballmaier M, Welte K (2007) Incidence of CSF3R mutations in severe congenital neutropenia and relevance for leukemogenesis: Results of a long-term survey. *Blood* 109(1):93–99.
13. Ma F, et al. (2007) Novel method for efficient production of multipotential hematopoietic progenitors from human embryonic stem cells. *Int J Hematol* 85(5):371–379.
14. Konishi N, et al. (1999) Defective proliferation of primitive myeloid progenitor cells in patients with severe congenital neutropenia. *Blood* 94(12):4077–4083.
15. Nakamura K, et al. (2000) Abnormalities of primitive myeloid progenitor cells expressing granulocyte colony-stimulating factor receptor in patients with severe congenital neutropenia. *Blood* 96(13):4366–4369.
16. Skokowa J, Fobiwe JP, Dan L, Thakur BK, Welte K (2009) Neutrophil elastase is severely down-regulated in severe congenital neutropenia independent of ELA2 or HAX1 mutations but dependent on LEF-1. *Blood* 114(14):3044–3051.
17. Kawaguchi H, et al. (2003) Dysregulation of transcriptions in primary granule constituents during myeloid proliferation and differentiation in patients with severe congenital neutropenia. *J Leukoc Biol* 73(2):225–234.
18. Köllner I, et al. (2006) Mutations in neutrophil elastase causing congenital neutropenia lead to cytoplasmic protein accumulation and induction of the unfolded protein response. *Blood* 108(2):493–500.
19. Grenda DS, et al. (2007) Mutations of the ELA2 gene found in patients with severe congenital neutropenia induce the unfolded protein response and cellular apoptosis. *Blood* 110(13):4179–4187.
20. Pabst T, et al. (2001) AML1-ETO downregulates the granulocytic differentiation factor C/EBPalpha in t(8;21) myeloid leukemia. *Nat Med* 7(4):444–451.
21. Hirai H, et al. (2006) C/EBPbeta is required for 'emergency' granulopoiesis. *Nat Immunol* 7(7):732–739.
22. Bedi R, Du J, Sharma AK, Gomes I, Ackerman SJ (2009) Human C/EBP-ε activator and repressor isoforms differentially reprogram myeloid lineage commitment and differentiation. *Blood* 113(2):317–327.
23. Friedman AD (2007) Transcriptional control of granulocyte and monocyte development. *Oncogene* 26(47):6816–6828.
24. Hetz C (2012) The unfolded protein response: Controlling cell fate decisions under ER stress and beyond. *Nat Rev Mol Cell Biol* 13(2):89–102.
25. Skokowa J, et al. (2006) LEF-1 is crucial for neutrophil granulocytopoiesis and its expression is severely reduced in congenital neutropenia. *Nat Med* 12(10):1191–1197.
26. Mempel K, Pietsch T, Menzel T, Zeidler C, Welte K (1991) Increased serum levels of granulocyte colony-stimulating factor in patients with severe congenital neutropenia. *Blood* 77(9):1919–1922.
27. Nakahata T, Ogawa M (1982) Hemopoietic colony-forming cells in umbilical cord blood with extensive capability to generate mono- and multipotential hemopoietic progenitors. *J Clin Invest* 70(6):1324–1328.

blood

2012 119: 5458-5466
Prepublished online April 19, 2012;
doi:10.1182/blood-2011-05-354167

Frequent somatic mosaicism of *NEMO* in T cells of patients with X-linked anhidrotic ectodermal dysplasia with immunodeficiency

Tomoki Kawai, Ryuta Nishikomori, Kazushi Izawa, Yuuki Murata, Naoko Tanaka, Hidemasa Sakai, Megumu Saito, Takahiro Yasumi, Yuki Takaoka, Tatsutoshi Nakahata, Tomoyuki Mizukami, Hiroyuki Nunoi, Yuki Kiyohara, Atsushi Yoden, Takuji Murata, Shinya Sasaki, Etsuro Ito, Hiroshi Akutagawa, Toshinao Kawai, Chihaya Imai, Satoshi Okada, Masao Kobayashi and Toshio Heike

Blood (print ISSN 0006-4971, online ISSN 1528-0020), is published weekly by the American Society of Hematology, 2021 L St, NW, Suite 900, Washington DC 20036.

Frequent somatic mosaicism of *NEMO* in T cells of patients with X-linked anhidrotic ectodermal dysplasia with immunodeficiency

Tomoki Kawai,[1] Ryuta Nishikomori,[1] Kazushi Izawa,[1] Yuuki Murata,[1] Naoko Tanaka,[1] Hidemasa Sakai,[1] Megumu Saito,[2] Takahiro Yasumi,[1] Yuki Takaoka,[1] Tatsutoshi Nakahata,[2] Tomoyuki Mizukami,[3] Hiroyuki Nunoi,[3] Yuki Kiyohara,[4] Atsushi Yoden,[5] Takuji Murata,[5] Shinya Sasaki,[6] Etsuro Ito,[6] Hiroshi Akutagawa,[7] Toshinao Kawai,[8] Chihaya Imai,[9] Satoshi Okada,[10] Masao Kobayashi,[10] and Toshio Heike[1]

[1]Department of Pediatrics, Kyoto University Graduate School of Medicine, Kyoto, Japan; [2]Clinical Application Department, Center for iPS Cell Research and Application, Institute for Integrated Cell-Material Sciences, Kyoto University, Kyoto, Japan; [3]Division of Pediatrics, Department of Reproductive and Developmental Medicine, Faculty of Medicine, University of Miyazaki, Miyazaki, Japan; [4]Department of Pediatrics, Faculty of Medicine, Osaka University, Suita, Japan; [5]Department of Pediatrics, Osaka Medical College, Takatsuki, Japan; [6]Department of Pediatrics, Hirosaki University Graduate School of Medicine, Hirosaki, Japan; [7]Department of Pediatrics, Kishiwada City Hospital, Kishiwada, Japan; [8]Department of Human Genetics, National Center for Child Health and Development, Tokyo, Japan; [9]Department of Pediatrics, Niigata University, Niigata, Japan; and [10]Department of Pediatrics, Hiroshima University Graduate School of Biomedical Sciences, Hiroshima, Japan

Somatic mosaicism has been described in several primary immunodeficiency diseases and causes modified phenotypes in affected patients. X-linked anhidrotic ectodermal dysplasia with immunodeficiency (XL-EDA-ID) is caused by hypomorphic mutations in the *NF-κB essential modulator (NEMO)* gene and manifests clinically in various ways. We have previously reported a case of XL-EDA-ID with somatic mosaicism caused by a duplication mutation of the *NEMO* gene, but the frequency of somatic mosaicism of *NEMO* and its clinical impact on XL-EDA-ID is not fully understood. In this study, somatic mosaicism of *NEMO* was evaluated in XL-EDA-ID patients in Japan. Cells expressing wild-type NEMO, most of which were derived from the T-cell lineage, were detected in 9 of 10 XL-EDA-ID patients. These data indicate that the frequency of somatic mosaicism of *NEMO* is high in XL-ED-ID patients and that the presence of somatic mosaicism of *NEMO* could have an impact on the diagnosis and treatment of XL-ED-ID patients. (*Blood*. 2012;119(23):5458-5466)

Introduction

X-linked anhidrotic ectodermal dysplasia with immunodeficiency (XL-EDA-ID) is a disease with clinical features including hypohidrosis, delayed eruption of teeth, coarse hair, and immunodeficiency associated with frequent bacterial infections.[1-5] The gene responsible for XL-EDA-ID has been identified as *NF-κB essential modulator (NEMO)*.[6-8] NEMO is necessary for the function of IκB kinase, which phosphorylates and degrades IκB to activate NF-κB.[9-10] Defects in NEMO cause various abnormalities in signal transduction pathways involving NF-κB, and affect factors such as the IL-1 family protein receptors, the TLRs, VEGFR-3, receptor activator of nuclear factor κB (RANK), the ectodysplasin-A receptor, CD40, and the TNF receptor I.[7] Whereas a complete loss of NEMO function in humans is believed to cause embryonic lethality,[11] *NEMO* mutations in XL-EDA-ID patients are hypomorphic,[8] causing a partial loss of NEMO functions.

In XL-EDA-ID, NEMO defects lead to diverse immunologic features including susceptibility to pathogens, impaired Ab response to polysaccharides,[2,4,12] hypogammaglobulinemia,[13] hyper IgM syndrome,[14] and impaired NK-cell activity,[15] with a large degree of variability in phenotypes among the patients. For example, approximately one-tenth of XL-EDA-ID patients exhibit reduced mitogen-induced proliferation of T lymphocytes.[12] Moreover, one-fourth suffer from inflammatory disorders such as inflammatory bowel disease and rheumatoid arthritis,[12] although the inflammatory process usually relies on NF-κB activation.[16] One explanation for this clinical variability is that the XL-EDA-ID phenotype is *NEMO* genotype-specific. Although the XL-EDA-ID database reported by Hanson et al succeeds to some extent in linking the specific clinical features to *NEMO* genotype,[12] the penetrance of some clinical features is not high and the mechanism accounting for this variability is unknown.

Recently, we have reported a case of spontaneous reversion mosaicism of the *NEMO* gene in XL-EDA-ID, which showed an atypical phenotype involving decreased mitogen-induced T-cell proliferation along with decreased CD4 T cells (patient 1).[17] There have been no subsequent reports on somatic mosaicism in XL-EDA-ID, and its prevalence and impact on the clinical features of the disease is unknown. In this study, we describe the younger brother of patient 1, who suffered from XL-EDA-ID with the same mutation and somatic reversion mosaicism of *NEMO*. Patient 2 showed intriguing laboratory findings in that mitogen-induced T-cell proliferation varied in accordance with the rate of detected reversion in the peripheral blood. These 2 cases led us to perform a nationwide study of XL-EDA-ID patients in Japan that revealed a high incidence of somatic mosaicism of *NEMO*.

Submitted May 11, 2011; accepted April 8, 2012. Prepublished online as *Blood* First Edition paper, April 19, 2012; DOI 10.1182/blood-2011-05-354167.

The online version of this article contains a data supplement.

The publication costs of this article were defrayed in part by page charge payment. Therefore, and solely to indicate this fact, this article is hereby marked "advertisement" in accordance with 18 USC section 1734.

Table 1. Clinical and genetic features of XL-EDA-ID patients

Patient	Mutation	Ectodermal dysplasia	Mitogen-induced proliferation	Infections	Complications	Therapy	Sex chromosome chimerism
1	Duplication	+	Reduced	Sepsis (S.P. and P.A.)	Chronic diarrhea	IVIG	100% XY
				Disseminated M.A.C.	Failure to thrive	RFP, CAM, AMK, EB	
				Skin abscess (S.A.)	Small intestinal stenosis	Rifabutin	
				Invasive *Aspergillus*	Lymphedema		
2	Duplication	+	Reduced	Sepsis (*E coli*)	Failure to thrive	IVIG, ST, EB, CAM	99.8% XY 0.2% X
				Disseminated M.S.		Rifabutin, SCT	
3	D311E	−	Normal	Disseminated B.C.G.		IVIG, INH	100% XY
				Sepsis (S.P.)		RFP, SCT	
4	A169P	+	Normal	Meningitis (S.P.)	IBD	IVIG, ST, PSL	99% XY
					Interstitial pneumonia	CyA, MTX, Infliximab	
					Rheumatoid arthritis		
5	L227P	+	Normal	Recurrent pneumonia	IBD	ST, mesalazine	Not done
				Pyogenic coxitis		Infliximab	
				Recurrent otitis media			
6	R182P	+	Not done	Recurrent otitis media	IBD	ST, mesalazine	99.8% XY 0.2% X
				UTI, Recurrent stomatitis			
				Subepidermal abscess			
7	R175P	+	Normal	Recurrent sepsis (S.P.)		IVIG	100% XY
8	Q348X	+	Normal	Disseminated B.C.G.	IBD	IVIG, ST	100% XY
9	R175P	+	Normal	Recurrent pneumonia	IBD	IVIG	100% XY
				Recurrent otitis media		5-aminosalicylic acid	
				Kaposi varicelliform eruption			
10	1167 ins C	+	Normal	Sepsis and Enteritis (E.A)	Failure to thrive	IVIG, SCT	Not done
				Sepsis (C.G.)	Pyloric stenosis, colon polyps		
				UTI (K.P.)			

S.P. indicates *Streptococcus pneumoniae*; P.A., *Pseudomonas aeruginosa*; IVIG, intravascular immunoglobulin infusion; M.A.C., *Mycobacterium avium* complex; S.A., *Staphylococcus aureus*; *E coli*, *Escherichia coli*; ST, trimethoprim-sulfamethoxazole; M.S., *Mycobacterium szulgai*; AMK, amikacin; EB, ethambutol; CAM, clarithromycin; SCT, stem cell transplantation; B.C.G., Bacille de Calmette et Guerin; INH, isoniazid; RFP, rifampicin; IBD, inflammatory bowel disease; PSL, prednisolone; CyA, cyclosporine A; MTX, methotrexate; UTI, urinary tract infection; E.A., *Enterobacter aerogenes*; C.G., *Candida glabrata*; and K.P., *Klebsiella* pneumonia.

Methods

Informed consent

Informed consent was obtained from the patients and their families following the Declaration of Helsinki according to the protocol of the Internal Review Board of Kyoto University, which approved this study.

Patients

Patient 1 was an XL-EDA-ID patient with a duplication mutation of the *NEMO* gene spanning intron 3 to exon 6. This patient has been reported previously[17] and died from an *Aspergillus* infection at the age of 4. Patient 2, born at term, was the younger brother of patient 1. This patient was also diagnosed as XL-EDA-ID with the same duplication mutation as patient 1 by genetic study. He received trimethoprim-sulfamethoxazole prophylaxis and a monthly infusion of immunoglobulin from the age of 1 month. The patient maintained good health and had a body weight of 7899*g* at 6 months when he started to fail to thrive. Except for poor weight gain, patient 2 appeared active with a good appetite, negative C-reactive protein, normal white blood cell counts, and no apparent symptoms. At 19 months of age, *Mycobacterium szulgai* was detected by venous blood culture, and the patient was treated with multidrug regimens including ethambutol, rifabutin, and clarithromycin based on the treatment of systemic *Mycobacterium avium* complex infection. The patient responded well to the treatment and his weight increased from 7830*g* to 9165*g* within a month after the treatment was initiated. Patient 2 received an unrelated cord blood cell transplantation at 26 months of age, containing 8.5×10^7 nucleated cells/kg (4.4×10^5 $CD34^+$ cells/kg), which was matched at 5 of 8 loci: mismatches occurred at 1 HLA-B and 1 HLA-C allele (according to serology), and at 1 HLA-A, 1 HLA-B, and 1 HLA-C allele (according to DNA typing). The preconditioning regimen consisted of fludarabine (30 mg/m^2/d) on days −7 to −3, melphalan (70 mg/m^2/d) on days −6 to −5, and rabbit anti-thymocyte globulin (2.5 mg/kg/d) on days −6 to −2. At first, Tacrolimus (0.024 mg/kg/d) was used to prevent GVHD, but this was switched to cyclosporin A (3 mg/kg/d) on day 9 because of drug-induced encephalopathy. Neutrophil ($> 0.5 \times 10^9$/L) and platelet ($> 50 \times 10^9$/L) engraftment were examined on days 13 and 40, respectively. Although $CD19^+$ cells (2042/μL, 94% donor chimerism), $CD56^+$ cells (242/μL, 97% donor chimerism), and monocytes (557/μL, 69% donor chimerism) were successfully generated, $CD3^+$ cells were not detected in the peripheral blood by day 54. The patient suffered from septic shock and died on day 60. Patients 3 to 10 were XL-EDA-ID patients recruited nationwide in Japan. Clinical details of patients 3, 4, and 10 have been reported previously.[18-20] These patients had clinical phenotypes characteristic of XL-EDA-ID such as ectodermal dysplasia, innate and/or acquired immunity defects, and susceptibility to pyogenic bacteria and *Mycobacterium* infection. Every patient had a mutation in the *NEMO* gene that caused reduced NF-κB activation in a NEMO reconstitution assay, as described in "Proliferation of $NEMO^{normal}$ and $NEMO^{low}$ T cells." Patient profiles are listed in Table 1.

Flow cytometric analysis

NEMO intracellular staining was performed as previously described.[17] The cells were stained for the following lineage markers before staining for NEMO: CD4, CD8, CD14, CD15, CD19, CD56, CD45RA (BD Biosciences/BD Pharmingen), and CCR7 (R&D Systems Inc). Intracellular staining of human IFN-γ, TNF-α, and NEMO was performed as previously described.[18] The stained cells were collected using a FACSCalibur flow cytometer (BD Biosciences) and analyzed using the FlowJo software (TreeStar).

Reporter assay

Wild-type and mutant *NEMO* cDNAs were generated from a healthy volunteer and the recruited XL-EDA-ID patients by RT-PCR; the cDNAs were subcloned into the p3xFLAG-CMV14 vector (Sigma-Aldrich). NEMO null rat fibroblast cells (kindly provided by Dr S. Yamaoka, Department of Molecular Virology, Graduate School of Medicine, Tokyo Medical and Dental University, Tokyo, Japan) were plated at a density of

3×10^4 cells/well in a 24-well culture dish and were transfected with 40 ng of NF-κB reporter plasmid (pNF-κB-Luc; BD Biosciences/BD Clontech), 2 ng of *NEMO* mutant expression construct, 10 ng of internal control for the normalization of transfection efficiency (pRL-TK; Toyo Ink), and 148 ng of mock vector using FuGENE HD Transfection Reagent (TOYO-B-Net) according to the manufacturer's protocol. Twelve hours after transfection, the cells were stimulated with 15 ng/mL lipopolysaccharide (LPS; Sigma-Aldrich) for 4 hours and the NF-κB activity was measured using the PicaGene Dual SeaPansy assay kit (TOYO-B-Net). Experiments were performed in triplicate and firefly luciferase activity was normalized to *Renilla* luciferase activity.

Subcloning analysis of cDNA

Cell sorting of the various cell lineages was performed by FACSVantage (BD Biosciences). The purity of each lineage was > 95%. The cDNA from sorted cells was purified and reverse transcribed by Super Script III (Invitrogen) with random hexamers and amplified by the proofreading PCR enzyme KOD, as previously described.[17,21] The PCR primers used were NEMO2 (5′-AGAGACGAAGGAGCACAAAGCTGCCTTGAG-3′) and NEMO3 (5′-ACTGCAGGGACAATGGTGGGTGCATCTGTC-3′). The PCR products were subcloned using a TA cloning kit (Invitrogen) and sequenced by ABI 3130xl Genetic analyzer (Applied Biosystems). To determine whether additional mutations occurred in revertant subclones that had wild-type sequence in the original mutation site, the entire coding region of the *NEMO* gene was sequenced and an additional mutation was considered present when the same mutation was detected in multiple subclones.

Allele-specific PCR

The mRNA purified from sorted T cells and monocytes was reverse-transcribed by SuperScript III (Invitrogen) with the gene-specific primer NEMO2 and amplified by the proofreading PCR enzyme KOD (Toyobo) using the primers NEMO3 and NEMO 4 (5′-TGTGGACACGCAGTGAAACGTGGTCTGGAG-3′). The PCR products were used as templates for allele-specific PCRs with Ex Taq polymerase (Takara Bio). Mutant and wild-type *NEMO* DNA was generated from each NEMO expression plasmid, mixed at graded ratios, and used as controls. PCR conditions and primer sequences are listed in supplemental Table 1 (available on the *Blood* Web site; see the Supplemental Materials link at the top of the online article).

Proliferation of NEMO^{normal} and NEMO^{low} T cells

To obtain PHA-induced T-cell blasts, PBMCs were stimulated with PHA (1:100; Invitrogen) and cultured in RPMI 1640 supplemented with 5% FCS and recombinant human IL-2 (50 IU/mL; kindly provided by Takeda Pharmaceutical Company) at 37°C for 7 days. Subcloning analysis of the cDNA obtained from the T-cell blasts was performed as described in "Subcloning analysis of cDNA."

Results

Reversion mosaicism of NEMO occurred in siblings with similar immunologic phenotypes

We previously reported patient 1 with a duplication mutation of the *NEMO* gene spanning intron 3 to exon 6, who was diagnosed as XL-EDA-ID at 1 year of age after suffering from recurrent infections.[17] At first, genetic diagnosis of the patient was difficult because the expression of aberrant *NEMO* mRNA was masked by the expression of normal *NEMO* mRNA by the revertant cells. Flow cytometric analysis of intracellular NEMO expression revealed cells with normal (NEMO^{normal}) and reduced (NEMO^{low}) levels of NEMO expression, indicating the presence of reversion mosaicism of the *NEMO* gene, and further analysis revealed that the *NEMO* mutation was disease-causing. PCR across the mutated region and sequencing of the PCR products revealed a duplication extending from intron 3 to exon 6, which was confirmed by Southern blot analysis. Additional copy number analysis of the *NEMO* gene of patient 1 and his mother excluded the possibility of a complex chromosomal aberration such as multiple duplication of the *NEMO* gene (supplemental Figure 1). Furthermore, polymorphism analysis using variable number tandem repeats on NEMO^{normal} and NEMO^{low} cells from patient 1 revealed that these cells were derived from the same origin (supplemental Table 2), indicating that the *NEMO* gene mosaicism was less likely because of amalgamation. The genomic analysis of the NEMO^{normal} cells revealed a complete reversion of the *NEMO* gene with no additional mutations. The clinical phenotype of patient 1 was combined immunodeficiency with a reduced number of T cells and mitogen-induced proliferation (Tables 2-3). We previously determined that reduced NEMO expression in the mutant T cells caused impairment of T-cell development and mitogen-induced proliferation.

Patient 2, the younger brother of patient 1, was diagnosed as XL-EDA-ID with the same duplication mutation as his brother. Flow cytometric analysis of intracellular NEMO expression performed at diagnosis showed that most of his PBMCs had reduced NEMO expression (Figure 1A). At 2 months of age, when most of the T cells were NEMO^{low}, absolute counts of the patient's T cells and the mitogen-induced proliferation of the patient's PBMCs were comparable with those of the healthy controls (Figure 1A-B; Table 2). These findings indicated that the *NEMO* mutation had no effect on T-cell development and mitogen-induced proliferation during early infancy in patient 2.

NEMO^{normal} T cells gradually increased as patient 2 grew older, while the absolute count of NEMO^{low} T cells decreased (Figure 1A-B). Accordingly, normal full-length *NEMO* cDNA, which had been undetectable in cord blood, was detectable in the patient's peripheral blood at 12 months of age. However, while NEMO^{normal} T cells were increasing, mitogen-induced T-cell proliferation started to decrease (Table 3), and the patient started to show poor weight gain from 6 months of age. When patient 2 was 17 months old, a blood culture revealed an *M szulgai* bacteremia. At this time, the absolute count of NEMO^{normal} T cells peaked, and NEMO^{low} T cells were at a minimum. He began to gain weight after anti-*Mycobacterium* medication was initiated, although NEMO^{normal} T cells started to decrease and NEMO^{low} T cells began to increase (Figure 1B). When the patient was 23 months old, mitogen-induced T-cell proliferation was still low and a roughly equal number of NEMO^{low} and NEMO^{normal} T cells were detected (Table 3). Overall, as patient 2 grew older, NEMO^{normal} T cells increased as the total number of T cells and the mitogen-induced T-cell proliferation decreased, similar to what had occurred in patient 1 at a similar age.

Various analyses were performed to compare the immunologic phenotype of NEMO^{low} and NEMO^{normal} T cells in detail. Both NEMO^{normal} and NEMO^{low} CD4$^+$ T cells carried a diverse Vβ repertoire, but CD8$^+$ T cells had a skewed Vβ repertoire regardless of NEMO expression level (Figure 1C). Surface marker analysis revealed that most of the NEMO^{normal} T cells were CD45RA$^-$/CCR7$^-$ and most of the NEMO^{low} T cells were CD45RA$^+$/CCR7$^+$ (Figure 1D). The NEMO^{normal} T cells produced similar amounts of IFN-γ and TNF-α as healthy control cells, while the production of these cytokines were reduced in NEMO^{low} T cells (Figure 1E-F). Taken together, these data implied that the immunologic phenotype of T cells from patient 2 converged with that of patient 1 as patient 2 grew older.

Table 2. Surface marker analysis of peripheral mononuclear cells of patients 1 and 2

	Patient 1	Patient 2		Healthy controls
Age at analysis	2 y	2 mo	19 mo	
CD3	1503	2366	1014	2997 ± 1751
CD4	292	1583	374	1683 ± 874
CD8	1160	783	547	1114 ± 976
TCRαβ	1386	2295	439	2620 ± 1612
TCRγδ	109	74	574	343 ± 177
$CD4^+CD45RA$	58	1336	105	1471 ± 890
$CD4^+CD45RO$	263	307	266	497 ± 189
$CD8^+CD45RA$	1178	783	297	1083 ± 1078
$CD8^+CD45RO$	361	21	250	385 ± 442
$CD4^+CD25$	80	427	93	210 ± 99
CD19	1200	941	1543	1252 ± 1145
CD20	1189	931	1536	1125 ± 837
$CD19^+$Sm-IgG	7	18	17	54 ± 21
$CD19^+$Sm-IgA	15	4	14	18 ± 14
$CD19^+$Sm-IgM	1171	910	1505	1057 ± 881
$CD19^+$Sm-IgD	1171	906	1495	1052 ± 884
CD16	912	176	24	287 ± 200
CD56	908	176	24	306 ± 207

Surface markers expressed by XL-EDA-ID patients' PBMCs are shown as absolute counts per microliter of peripheral blood. Healthy control values are based on children aged 1 to 6 years and are shown as the mean ± SD.

Sm indicates the surface membrane.

High incidence of somatic mosaicism of the *NEMO* gene in XL-EDA-ID patients

It is worth noting that somatic reversion mosaicism of the *NEMO* gene occurred in both of the 2 XL-EDA-ID siblings carrying a duplication mutation. To determine whether a high frequency of reversion is a specific event for this type of *NEMO* duplication mutation[22-25] or if the reversion of the *NEMO* gene occurs commonly in XL-EDA-ID patients, we recruited an additional 8 XL-EDA-ID patients from throughout Japan (Table 1) and analyzed the presence of *NEMO* reversion. These patients had various combinations of clinical phenotypes characteristic of XL-EDA-ID such as ectodermal dysplasia, innate and acquired immunity defects, and susceptibility to pyogenic bacteria and *Mycobacterium* infections. Every patient had a mutation of the *NEMO* gene with reduced NF-κB activation potential, as evaluated in a NEMO reconstitution assay (Figure 2).

Among the 8 patients, only patient 3 had a large proportion of $NEMO^{low}$ cells by flow cytometric analysis. The majority of patient 3's PBMCs were $NEMO^{low}$, whereas 10% of the patient's $CD8^+$ cells were $NEMO^{normal}$ (Figure 3A). This patient was identified as carrying the D311E mutation. Because missense mutations of the *NEMO* gene often do not result in the reduced expression of NEMO protein, subcloning and sequencing analysis was performed on the *NEMO* cDNA isolated from the remaining patients, and 6 of the 7 patients had normal *NEMO* subclones (Table 3). Expansion of maternal cells after fetomaternal transfusion was ruled out in these patients by FISH analysis with X and Y probes (Table 1).

Additional genetic analysis of the entire coding region of the *NEMO* gene was performed on $NEMO^{normal}$ cells from patient 3 and on reverted subclones from the other patients, except for patient 10 who had already received stem cell transplantation. The *NEMO* gene in these samples had reverted to wild-type with no additional mutations (Figure 3B and data not shown). To specifically determine in which cell lineages the reversion occurred, subcloning and sequencing analysis of cDNA in various cell lineages was performed. This analysis revealed that all the revertant cells were of the T-cell lineage and that no reversion occurred in monocytes and very little occurred in B cells (Table 4). Allele-specific PCR confirmed that reversion occurred in T cells but not in monocytes (Figure 4).

Selective advantage of $NEMO^{normal}$ cells in XL-EDA-ID carriers

The high frequency of somatic mosaicism in T cells of XL-EDA-ID patients indicated a strong selective advantage of wild-type NEMO T cells over T cells carrying mutant NEMO. To confirm this hypothesis, *NEMO* cDNA analysis was performed on various cell lineages from the mothers of the patients who are heterozygous for *NEMO* mutation and thus have mosaicism

Table 3. Immunologic analysis of patients 1 and 2

	Patient 1	Patient 2 (treated with IVIG)	
Age at analysis, mo	9	9	20
Serum immunoglobulin levels, g/L (control)			
IgG	10.63 (4.51-10.46)	8.44 (4.51-10.46)	10.37 (7.15-9.07)
IgA	1.36 (0.14-0.64)	1.88 (0.14-0.64)	3.93 (0.22-1.44)
IgM	0.4 (0.33-1.00)	0.17 (0.33-1.00)	0.20 (0.34-1.28)
Age at analysis	2 y	2 mo	23 mo
T-cell proliferation, SI (control)	9.3 (206.9 ± 142.5)	55.3 (64.8 ± 8.1)	7.2 (89.4 ± 31.2)

Control values of serum immunoglobulin levels are based on children aged either 7 to 9 months or 1 to 2 years and are shown as the mean ± SD. The T-cell proliferation assay was performed as described previously[17] with at least three healthy adults as controls.

SI indicates stimulation index; and IVIG, 2.5 g of monthly IV immune globulin infusion.

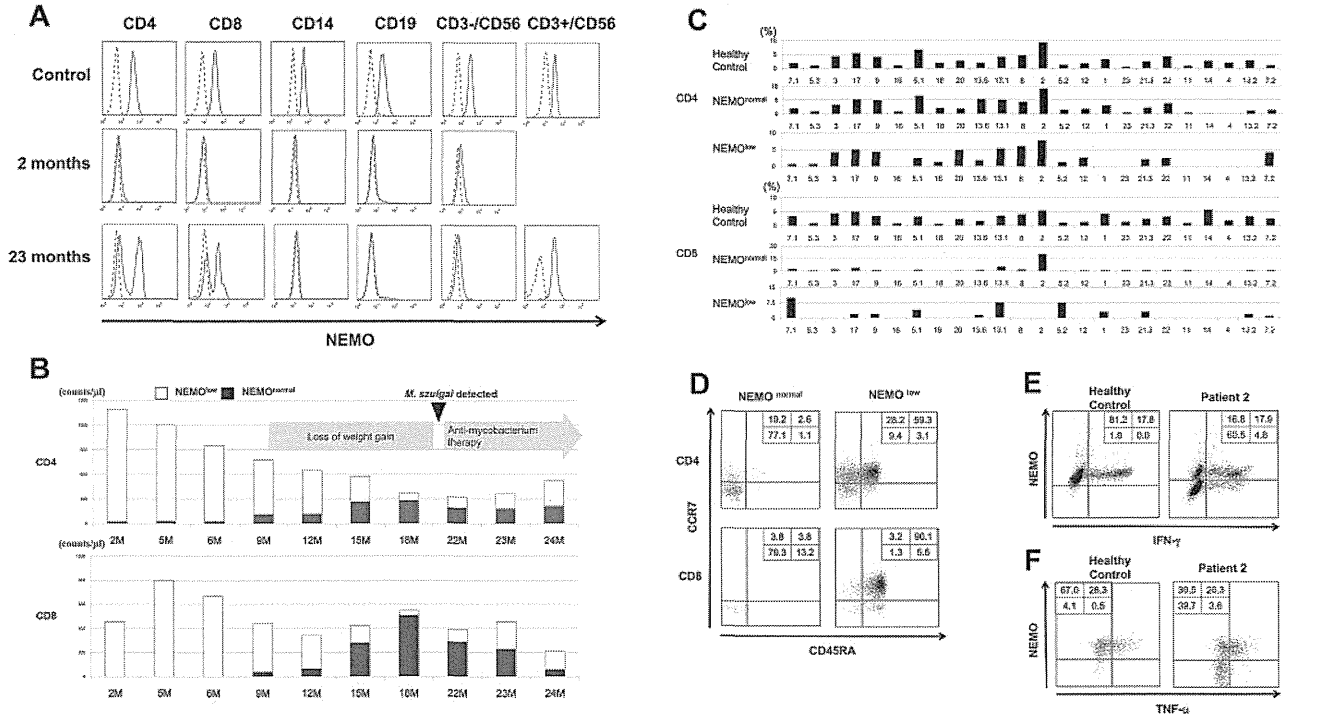

Figure 1. Identification and characterization of *NEMO* revertant T cells in patient 2. (A) Intracellular expression of NEMO in various PBMC lineages from a healthy adult control and patient 2 were evaluated by flow cytometry. For the patient, results of the analyses performed at 2 months and 23 months are shown. Solid lines indicate staining with the anti-NEMO mAb, and dotted lines indicate the isotype control. (B) Time-course variations in the absolute count of $NEMO^{normal}$ and $NEMO^{low}$ T cells in patient 2. M indicates age in months. (C) TCR-Vβ repertoire analysis of the patient's $CD4^+$ and $CD8^+$ T cells. PBMCs from the patient and a healthy adult control were stained for the TCR-Vβ panel, CD4, CD8, and NEMO, and analyzed by flow cytometry. (D) Phenotype analysis of T cells in patient 2. PBMCs from the patient and a control were stained for the expression of NEMO, CCR7, CD45RA, and CD4 or CD8. Data shown were gated on $NEMO^{normal}$ or $NEMO^{low}$ $CD4^+$ or $CD8^+$ cells. (E-F) Cytokine production from $NEMO^{normal}$ and $NEMO^{low}$ T cells. PBMCs from the patient and a control were stimulated with PMA and ionomycin for 6 hours and stained for intracellular (E) IFN-γ or (F) TNF-α along with NEMO. Cells shown are gated on the $CD3^+$ population.

because of X-chromosome inactivation. This analysis assumes that the percentage of cDNA for wild-type *NEMO* reflects the percentage of cells expressing wild-type NEMO. A high proportion of wild-type *NEMO* cDNA was observed in T cells from the mothers of patients 1/2, 3, 8, and 10, although wild-type *NEMO* cDNA was not predominant in T cells from the mother of patient 4 (Table 5).

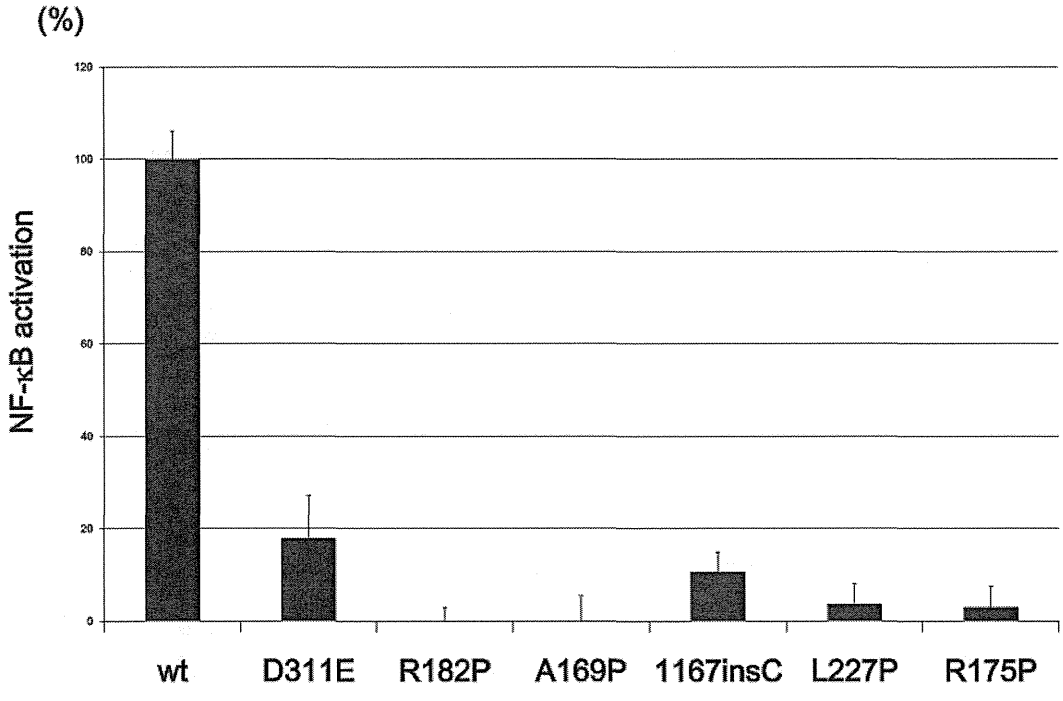

Figure 2. NF-κB transactivation by NEMO mutants from the XL-EDA-ID patients. NF-κB transactivation induced by NEMO mutants in the XL-EDA-ID patients. Mock vectors and wild-type (wt) NEMO were used as controls. The NF-κB activation index of NEMO variants were calculated as (NF-κB activation by each NEMO variant − NF-κB activation of the mock vector)/(NF-κB activation by wild-type NEMO − NF-κB activation of the mock vector). The data shown are the mean ± SD of triplicate wells and are representative of 3 independent experiments with similar results.

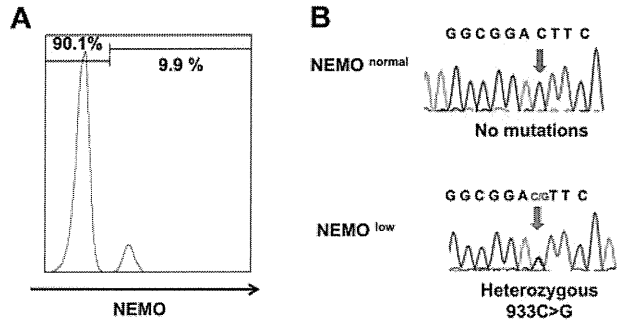

Figure 3. *NEMO* revertant T cells in patient 3. (A) Intracellular expression of NEMO in $CD8^+$ cells from patient 3. (B) Sequencing chromatograms of DNA from $NEMO^{normal}$ or $NEMO^{low}$ $CD8^+$ cells of patient 3. Arrows indicate the mutated base position at c. 931.

Similarly, there was an apparent high proportion of wild-type *NEMO* cDNA in monocytes and B cells from the mothers of patients 1/2, 8, and 10 (Table 5). These findings suggested a general selective advantage of $NEMO^{normal}$ cells over $NEMO^{low}$ cells in vivo, especially in T cells.

Proliferation capacity of $NEMO^{normal}$ and $NEMO^{low}$ T cells

T-cell proliferation stimulated by mitogens such as PHA is usually not reduced in XL-EDA-ID patients. However, the emergence of $NEMO^{normal}$ cells coincided with a reduction in mitogen-induced proliferation in patient 2. To further determine the effect of $NEMO^{normal}$ cells on mitogen-induced proliferation of peripheral T cells, the proportions of T cells carrying the wild-type and mutant were examined before and after PHA stimulation in XL-EDA-ID patients and their mothers (Table 6). In patients 2, 4, and 8, the percentage of the $NEMO^{normal}$ cells decreased after PHA stimulation, while $NEMO^{normal}$ cells prevailed in patient 9. In the mothers of patient 4 and 10, the percentage of $NEMO^{normal}$ cells increased after PHA stimulation, while the percentage of the $NEMO^{normal}$ cells decreased in the mother of patient 3. These results indicated that the NEMO mutation does not directly affect the mitogen-induced proliferation capacity of T cells and factors other than the *NEMO* genotype determine the proliferation capacity of $NEMO^{normal}$ and $NEMO^{low}$ T cells.

Discussion

Somatic reversion mosaicism has been described in several disorders affecting the hematopoietic system, the liver, and the skin.[23,26] Reports of somatic reversion cases have been particularly abundant in patients with immunodeficiency diseases, including Wiskott-Aldrich syndrome (WAS)[27] and SCID, which occur because of mutations in the interleukin receptor common γ chain,[28] CD3ζ,[29] *RAG-1*[30], and *ADA* genes.[31] Patients with somatic reversion mosaicism may present with significantly milder clinical phenotypes compared with nonrevertant patients with the same germline mutation, although this is not always the case.[26] One common feature in most cases where the somatic reversion mosaicism has been observed is a strong in vivo selective advantage of the revertant cells that express the wild-type gene product. One of the most intensively investigated diseases associated with somatic reversion mosaicism is WAS.[32-34] A report showed that up to 11% of WAS patients have presented with somatic reversion mosaicism.[33]

In our investigation, 9 of 10 XL-EDA-ID patients presented with somatic mosaicism. Two of the 9 were cases of reversion from a duplication mutation, while the others exhibited true back-reversion from a substitution or insertion mutation. This finding calls for caution when diagnosing XL-EDA-ID patients. Because the existence of a *NEMO* pseudogene makes it difficult to perform genetic analysis using genomic DNA, diagnosis of the disease is often confirmed by sequencing analysis of *NEMO* cDNA, and the presence of somatic mosaicism can cause misdiagnosis of XL-EDA-ID patients either when $NEMO^{normal}$ cells make up the majority of the patients' PBMCs or when the cDNA of the mutated *NEMO* gene cannot be amplified by PCR.[17] In fact, mutated *NEMO* cDNA could not be amplified from the PBMCs of patient 2 even when $NEMO^{normal}$ cells were absent (during early infancy), and only wild-type *NEMO* cDNA was amplified after the appearance of $NEMO^{normal}$ cells (data not shown), probably because of the instability of the mutated *NEMO* mRNA. Flow cytometric analysis of intracellular NEMO protein is of help in identifying the $NEMO^{low}$ cells in some patients, but the technique is not applicable when the *NEMO* mutation does not cause reduced expression of NEMO protein. Thus, some cases of XL-EDA-ID patients with reversion may be difficult to diagnose.

The high frequency of somatic mosaicism observed in XL-EDA-ID patients indicates a strong in vivo selective advantage for $NEMO^{normal}$ cells, which express the wild-type gene product. Patient 2 presented with a high mutant T-cell count at birth that gradually decreased over time (Figure 1B). This finding indicates that wild-type NEMO expression is critical for the survival of certain cell lineages, including T cells, after birth. On the other hand, no $NEMO^{normal}$ monocytes and very few $NEMO^{normal}$ B cells were detected in the recruited XL-EDA-ID patients (Table 4). This specific feature is similar to other somatic reversion mosaicism seen in primary immunodeficiency patients[26] and indicates that the expression of NEMO is less critical for the survival of monocytes or B cells compared with that of T cells. There is also an apparent

Table 4. Analysis of *NEMO* gene mosaicism in various cell lineages for each patient

Patient	Mutation	Age at analysis	CD4, % (proportion)	CD8, % (proportion)	CD14, % (proportion)	CD19, % (proportion)
1	Duplication	2 y	90	100	0	4.0
2	Duplication	15 mo	45	66	0	4.0
3	D311E	3 y	2.4	9.9	0	1.2
4	A169P	12 y	0 (0/19)	24 (9/37)	0 (0/19)	0 (0/47)
5	L227P	3 y	0 (0/25)	0 (0/35)	0 (0/30)	0 (0/25)
6	R182P	4 y	18 (5/28)	17 (9/52)	0 (0/27)	0 (0/33)
7	R175P	6 y	0.4 (1/25)	39 (11/28)	0 (0/28)	0 (0/25)
8	Q348X	8 y	38 (6/16)	47 (9/19)	0 (0/33)	0 (0/25)
9	R175P	15 y	30 (9/30)	36 (12/33)	0 (0/23)	0 (0/14)
10	1167 ins C	9 mo	PBMC 9.3 (4/43)			

For patients 1 to 3, data represent the percentages of $NEMO^{normal}$ cells in each lineage, as assessed by flow cytometry. For patients 4 to 10, the ratio indicates the number of wild-type NEMO clones in various cell lineages as compared with the total number of clones analyzed, based on subcloning and sequencing analysis.

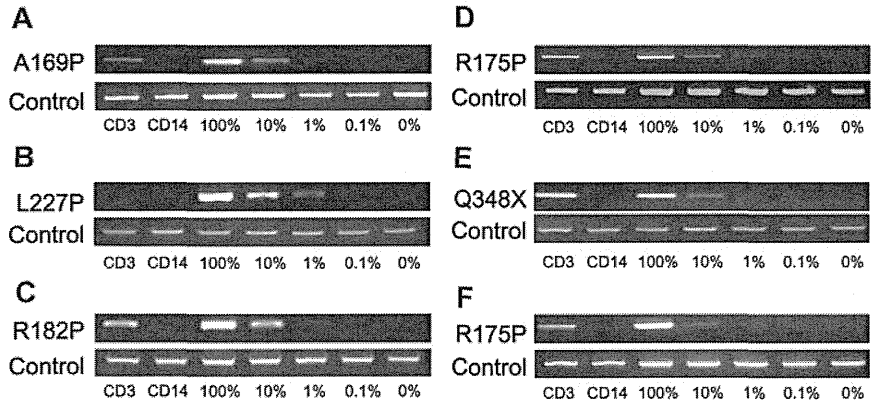

Figure 4. NEMO reversion selectively occurs in T cells of XL-EDA-ID patients. Allele-specific PCR for *NEMO* on CD3$^+$ or CD14$^+$ cells from (A) patient 4, (B) patient 5, (C) patient 6, (D) patient 7, (E) patient 8, and (F) patient 9. Numbers below each figure indicate the percentages of wild-type NEMO cDNA mixed with each mutant. Primers used in each PCR are shown on the left.

concordance between the degree of the disruption of *NEMO* gene and the proportion of reverted NEMO^{normal} cells compared with NEMO^{low} cells. The high proportion of reverted T cells seen in patients 1 and 2 as well as in patient 8 was associated with a highly disruptive mutation of the *NEMO* gene (ie, a duplication mutation in patients 1 and 2, and a truncation mutation in patient 8). In addition, the highly selective X-chromosome inactivation observed in the mothers of XL-EDA-ID patients indicated a strong selective advantage for NEMO^{normal} cells over NEMO^{low} cells. It is also noteworthy that reverted T cells were not detected in patient 5, who carried an L227P mutation that was not localized to either of the functional domains in the NEMO protein. Other reported cases with the same mutation presented with polysaccharide-specific humoral immunodeficiency and autoinflammatory diseases, but were spared complications such as cellular immunodeficiency and susceptibility to *Mycobacterium* (similar to patient 5).[4,8] This may reflect the fact that the L227P mutation in NEMO has less influence on T-cell growth than NEMO mutations that occur in functional domains, and suggests that reversion of the mutation has little impact on T-cell survival. Although the number of cases in our study is limited, it appears that the more disruptive NEMO mutations favor the survival of NEMO^{normal} cells after reversion and X-chromosome inactivation.

Regarding the gradual decline in the number of NEMO-deficient T cells, one candidate trigger could be infection. Because the dominance of the memory phenotype and the skewed TCR repertoire among CD8$^+$ T cells in NEMO^{normal} cells were observed in both patients 1 and 2 (Figure 1C and Mizukami et al[18]), continuous infection of pyogenic bacteria in patient 1 and *M szulgai* in patient 2 could be a reason for the emergence of NEMO^{normal} cells and the elimination of NEMO^{low} cells. The decrease in NEMO^{normal} cells and restoration of NEMO^{low} cells after anti-mycobacterial therapy in patient 2 support this hypothesis. In the case of patient 1, the predominance of NEMO^{normal} T cells with an effector/memory phenotype at diagnosis (Table 4 and Mizukami et al[18]) is likely to be the result of chronic infection, and it is possible that NEMO^{low} cells were predominant during his early infancy. Because some reports have indicated that TNF-α–induced programmed cell death of several cell types, including a human T-cell line, was enhanced by hypomorphic *NEMO* mutations,[12,35] and considering our finding that the levels of TNF-α expressed in revertant T cells were similar to levels in healthy control T cells in vitro (Figure 1F), TNF-α produced from these cells in response to infection could be involved in mutant T-cell elimination.

Unexpectedly, T-cell proliferation in patient 2 was equivalent to that of normal controls at the age of 2 months and was reduced after NEMO^{normal} T cells increased (Figure 1B; Table 3). This finding indicates that the NEMO^{low} T cells did not have intrinsically impaired mitogen-induced proliferation. One reasonable explanation for the reduced proliferation observed after the increase in NEMO^{normal} T cells is a reduction in the absolute number of T cells (naive T cells in particular), probably because of the infection.

Table 5. Expression of mutant NEMO in various cell lineages for the mother of each XL-EDA-ID patient

Sample	Mutation	Analysis	Subtype	Mutant type, % (proportion)
Mother of patients 1 and 2	Duplication	FACS	CD3	0
			CD14	0
			CD19	0
Mother of patient 3	D311E	FACS	CD3	13
			CD3$^-$	54
		Subcloning	CD3	22 (6/27)
			CD3$^-$	55 (12/22)
Mother of patient 4	A169P	Subcloning	CD3	52 (11/21)
			CD14	58 (11/19)
			CD19	42 (5/12)
Mother of patient 8	Q348X	Subcloning	CD3	0 (0/26)
			CD14	17 (3/18)
			CD19	0 (0/18)
Mother of patient 10	1167insC	Subcloning	CD3	18 (7/39)
			CD14	12 (5/43)
			CD19	27 (12/44)

Data are shown as either the percentages of NEMO^{normal} cells, as assessed by flow cytometry, or as the ratio of clones containing wild-type NEMO to the total number of clones, as analyzed by subcloning and sequencing analysis.

Table 6. Expression of mutant NEMO in CD3-positive cells and PHA blasts

Sample	Mutations	Analysis	Subtype	Mutant type, % (proportion)
Mother of patient 3	D311E	FACS	CD3	13
			PHA blast	47
		Subcloning	CD3	22 (6/27)
			PHA blast	48 (11/23)
Mother of patient 4	A169P	Subcloning	CD3	52 (11/21)
			PHA blast	18 (9/49)
Mother of patient 8	Q348X	Subcloning	CD3	0 (0/26)
			PHA blast	0 (0/21)
Mother of patient 10	1167insC	Subcloning	CD3	18 (7/39)
			PHA blast	9 (4/43)
Patient 2	Duplication	FACS	CD3	73
			PHA blast	93
Patient 4	A169P	Subcloning	CD3	79 (19/24)
			PHA blast	100 (37/37)
Patient 8	Q348X	Subcloning	CD3	56 (18/32)
			PHA blast	100 (16/16)
Patient 9	R175P	Subcloning	CD3	87 (34/39)
			PHA blast	0 (0/28)

PHA blasts were obtained by incubating PBMCs with PHA and soluble IL-2 for 7 days. Data are shown as either the percentages of $NEMO^{normal}$ cells, as assessed by flow cytometry, or as the ratio of clones containing wild-type NEMO to the total number of clones, as analyzed by subcloning and sequencing analysis.

Therefore, to identify other mechanisms underlying reduced T-cell proliferation, the impact of *NEMO* mutation on PHA-induced T-cell proliferation was indirectly examined in vitro by comparing the response of $NEMO^{normal}$ and $NEMO^{low}$ cells derived from XL-EDA-ID patients and their mothers. After PHA stimulation and proliferation, the proportion of $NEMO^{low}$ T cells increased in patients 2, 4, and 8, while the opposite result was observed in patient 9 and in the mother of patient 4 (Table 6). Although the precise mechanism is unclear, a reduction in the proportion of $NEMO^{normal}$ cells after PHA stimulation would reflect the lower proliferative capacity of $NEMO^{normal}$ cells compared with that of $NEMO^{low}$ cells, which may be another explanation for the reduced T-cell proliferation observed in patient 2 at 23 months of age when $NEMO^{normal}$ T cells were dominant. In the reports on reversion mosaicism of *IL2RG* gene mutations,[28,36] the restoration of T-cell function and clinical symptoms varied among patients. Therefore, other factors besides the genotype of the mutations, such as the developmental stage where reversion occurred and the frequency of reversion, affect the clinical impact of somatic mosaicism of *NEMO* gene mutations.

In this study, the effect of somatic mosaicism of the *NEMO* gene on clinical phenotype could not be fully evaluated. However, cytokines produced by revertant T cells could influence the development of clinical symptoms of XL-EDA-ID, such as inflammatory bowel disease. In a mouse model, intestinal epithelial cell-specific inhibition of NF-κB through the conditional ablation of NEMO resulted in the development of chronic bowel inflammation sensitized intestinal epithelial cells to TNF-α–induced apoptosis.[37] In this model, the first phase of intestinal inflammation was initiated by epithelial cell death and was followed by a second phase of TNF-α–induced intestinal inflammation, the latter being dependent on T cells. Another report showed that HSCT in XL-EDA-ID patients exacerbated the patients' inflammatory bowel disease.[38] Indeed, in patient 4, the percentage of reverted T cells was reduced after repeated administrations of anti-TNFα blocking Ab, and the symptoms of inflammatory bowel disease improved.[18] Considering this evidence, somatic mosaicism in T cells might be an important factor leading to inflammatory disease in XL-EDA-ID patients with defective NF-κB activation. However, our study did not show a tight association between inflammatory bowel disease and somatic mosaicism, and further investigation is needed to determine whether the $NEMO^{normal}$ T cells play a role in inflammatory processes in XL-EDA-ID.

In conclusion, this study has identified a high frequency of somatic mosaicism in XL-EDA-ID patients, particularly in T cells, and has revealed important insights into human T-cell immunobiology in XL-EDA-ID. Although we could not demonstrate the clinical impact of somatic mosaicism in XL-EDA-ID patients, our findings suggest that care is required when making molecular diagnoses of XL-EDA-ID, and might shed light on the mechanisms underlying the variability in the clinical manifestation of XL-ED-ID and facilitate the search for appropriate treatments.

Acknowledgments

The authors are grateful to all the XL-EDA-ID patients and their families for their participation. They also thank Shoji Yamaoka (Department of Molecular Virology, Graduate School of Medicine, Tokyo Medical and Dental University, Tokyo, Japan) for kindly providing NEMO-null rat fibroblast cells, and Takeda Pharmaceutical Company Limited for kindly providing the recombinant human IL-2.

This work was supported by grants from the Japanese Ministry of Education, Culture, Sports, Science, and Technology, and by grants from the Japanese Ministry of Health, Labor and Welfare.

Authorship

Contribution: Tomoki Kawai wrote the manuscript and performed research; R.N., T.Y., T.N., and T.H. edited the manuscript and supervised this work; K.I., Y.M., N.T., H.S., M.S., and Y.T. cultured cells; and T. Mizukami, H.N., Y.K., A.Y., T. Murata, S.S., E.I., H.A., Toshinao Kawai, C.I., S.O., and M.K. treated patients and analyzed data.

Conflict-of-interest disclosure: The authors declare no competing financial interests.

Correspondence: Ryuta Nishikomori, MD, PhD, Department of Pediatrics, Kyoto University Graduate School of Medicine, 54 Kawahara-cho, Shogoin, Sakyo-ku, Kyoto 606-8507, Japan; e-mail: rnishiko@kuhp.kyoto-u.ac.jp.

References

1. Pinheiro M, Freire-Maia N. Ectodermal dysplasias: a clinical classification and a causal review. *Am J Med Genet.* 1994;53(2):153-162.
2. Abinun M, Spickett G, Appleton AL, Flood T, Cant AJ. Anhidrotic ectodermal dysplasia associated with specific antibody deficiency. *Eur J Pediatr.* 1996;155(2):146-147.
3. Sitton JE, Reimund EL. Extramedullary hematopoiesis of the cranial dura and anhidrotic ectodermal dysplasia. *Neuropediatrics.* 1992;23(2):108-110.
4. Schweizer P, Kalhoff H, Horneff G, Wahn V, Diekmann L. [Polysaccharide specific humoral immunodeficiency in ectodermal dysplasia. Case report of a boy with two affected brothers]. *Klin Padiatr.* 1999;211(6):459-461.
5. Abinun M. Ectodermal dysplasia and immunodeficiency. *Arch Dis Child.* 1995;73(2):185.
6. Zonana J, Elder ME, Schneider LC, et al. A novel X-linked disorder of immune deficiency and hypohidrotic ectodermal dysplasia is allelic to incontinentia pigmenti and due to mutations in IKK-gamma (NEMO). *Am J Hum Genet.* 2000;67(6):1555-1562.
7. Courtois G, Smahi A, Israel A. NEMO/IKK gamma: linking NF-kappa B to human disease. *Trends Mol Med.* 2001;7(10):427-430.
8. Doffinger R, Smahi A, Bessia C, et al. X-linked anhidrotic ectodermal dysplasia with immunodeficiency is caused by impaired NF-kappaB signaling. *Nat Genet.* 2001;27(3):277-285.
9. Rothwarf DM, Zandi E, Natoli G, Karin M. IKK-gamma is an essential regulatory subunit of the IkappaB kinase complex. *Nature.* 1998;395(6699):297-300.
10. Yamaoka S, Courtois G, Bessia C, et al. Complementation cloning of NEMO, a component of the IkappaB kinase complex essential for NF-kappaB activation. *Cell.* 1998;93(7):1231-1240.
11. Smahi A, Courtois G, Vabres P, et al. Genomic rearrangement in NEMO impairs NF-kappaB activation and is a cause of incontinentia pigmenti. The International Incontinentia Pigmenti (IP) Consortium. *Nature.* 2000;405(6785):466-472.
12. Hanson EP, Monaco-Shawver L, Solt LA, et al. Hypomorphic nuclear factor-kappaB essential modulator mutation database and reconstitution system identifies phenotypic and immunologic diversity. *J Allergy Clin Immunol.* 2008;122(6):1169-1177.
13. Orange JS, Jain A, Ballas ZK, Schneider LC, Geha RS, Bonilla FA. The presentation and natural history of immunodeficiency caused by nuclear factor kappaB essential modulator mutation. *J Allergy Clin Immunol.* 2004;113(4):725-733.
14. Jain A, Ma CA, Liu S, Brown M, Cohen J, Strober W. Specific missense mutations in NEMO result in hyper-IgM syndrome with hypohydrotic ectodermal dysplasia. *Nat Immunol.* 2001;2(3):223-228.
15. Orange JS, Brodeur SR, Jain A, et al. Deficient natural killer cell cytotoxicity in patients with IKK-gamma/NEMO mutations. *J Clin Invest.* 2002;109(11):1501-1509.
16. Sebban H, Courtois G. NF-kappaB and inflammation in genetic disease. *Biochem Pharmacol.* 2006;72(9):1153-1160.
17. Nishikomori R, Akutagawa H, Maruyama K, et al. X-linked ectodermal dysplasia and immunodeficiency caused by reversion mosaicism of NEMO reveals a critical role for NEMO in human T-cell development and/or survival. *Blood.* 2004;103(12):4565-4572.
18. Mizukami T, Obara M, Nishikomori R, et al. Successful treatment with infliximab for inflammatory colitis in a patient with X-linked anhidrotic ectodermal dysplasia with immunodeficiency. *J Clin Immunol.* 2012;32(1):39-49.
19. Imamura M, Kawai T, Okada S, et al. Disseminated BCG infection mimicking metastatic nasopharyngeal carcinoma in an immunodeficient child with a novel hypomorphic NEMO mutation. *J Clin Immunol.* 2011;31(5):802-810.
20. Tono C, Takahashi Y, Terui K, et al. Correction of immunodeficiency associated with NEMO mutation by umbilical cord blood transplantation using a reduced-intensity conditioning regimen. *Bone Marrow Transplant.* 2007;39(12):801-804.
21. Saito M, Nishikomori R, Kambe N, et al. Disease-associated CIAS1 mutations induce monocyte death, revealing low-level mosaicism in mutation-negative cryopyrin-associated periodic syndrome patients. *Blood.* 2008;111(4):2132-2141.
22. Yang TP, Stout JT, Konecki DS, Patel PI, Alford RL, Caskey CT. Spontaneous reversion of novel Lesch-Nyhan mutation by HPRT gene rearrangement. *Somat Cell Mol Genet.* 1988;14(3):293-303.
23. Zhang LH, Jenssen D. Reversion of the hprt mutant clone SP5 by intrachromosomal recombination. *Carcinogenesis.* 1992;13(4):609-615.
24. Monnat RJ Jr, Chiaverotti TA, Hackmann AF, Maresh GA. Molecular structure and genetic stability of human hypoxanthine phosphoribosyltransferase (HPRT) gene duplications. *Genomics.* 1992;13(3):788-796.
25. Rautenstrauss B, Liehr T, Fuchs C, et al. Mosaicism for Charcot-Marie-Tooth disease type 1A: onset in childhood suggests somatic reversion in early developmental stages. *Int J Mol Med.* 1998;1(2):333-337.
26. Wada T, Candotti F. Somatic mosaicism in primary immune deficiencies. *Curr Opin Allergy Clin Immunol.* 2008;8(6):510-514.
27. Ariga T, Kondoh T, Yamaguchi K, et al. Spontaneous in vivo reversion of an inherited mutation in the Wiskott-Aldrich syndrome. *J Immunol.* 2001;166(8):5245-5249.
28. Stephan V, Wahn V, Le Deist F, et al. Atypical X-linked severe combined immunodeficiency due to possible spontaneous reversion of the genetic defect in T cells. *N Engl J Med.* 1996;335(21):1563-1567.
29. Rieux-Laucat F, Hivroz C, Lim A, et al. Inherited and somatic CD3zeta mutations in a patient with T-cell deficiency. *N Engl J Med.* 2006;354(18):1913-1921.
30. Wada T, Toma T, Okamoto H, et al. Oligoclonal expansion of T lymphocytes with multiple second-site mutations leads to Omenn syndrome in a patient with RAG1-deficient severe combined immunodeficiency. *Blood.* 2005;106(6):2099-2101.
31. Hirschhorn R. In vivo reversion to normal of inherited mutations in humans. *J Med Genet.* 2003;40(10):721-728.
32. Wada T, Schurman SH, Jagadeesh GJ, Garabedian EK, Nelson DL, Candotti F. Multiple patients with revertant mosaicism in a single Wiskott-Aldrich syndrome family. *Blood.* 2004;104(5):1270-1272.
33. Stewart DM, Candotti F, Nelson DL. The phenomenon of spontaneous genetic reversions in the Wiskott-Aldrich syndrome: a report of the workshop of the ESID Genetics Working Party at the XIIth Meeting of the European Society for Immunodeficiencies (ESID). Budapest, Hungary October 4-7, 2006. *J Clin Immunol.* 2007;27(6):634-639.
34. Davis BR, Yan Q, Bui JH, et al. Somatic mosaicism in the Wiskott-Aldrich syndrome: molecular and functional characterization of genotypic revertants. *Clin Immunol.* 2010;135(1):72-83.
35. Yamaoka S, Inoue H, Sakurai M, et al. Constitutive activation of NF-kappa B is essential for transformation of rat fibroblasts by the human T-cell leukemia virus type I Tax protein. *EMBO J.* 1996;15(4):873-887.
36. Speckmann C, Pannicke U, Wiech E, et al. Clinical and immunologic consequences of a somatic reversion in a patient with X-linked severe combined immunodeficiency. *Blood.* 2008;112(10):4090-4097.
37. Nenci A, Becker C, Wullaert A, et al. Epithelial NEMO links innate immunity to chronic intestinal inflammation. *Nature.* 2007;446(7135):557-561.
38. Fish JD, Duerst RE, Gelfand EW, Orange JS, Bunin N. Challenges in the use of allogeneic hematopoietic SCT for ectodermal dysplasia with immune deficiency. *Bone Marrow Transplant.* 2009;43(3):217-221.

bjh research paper

Identification of the integrin β3 L718P mutation in a pedigree with autosomal dominant thrombocytopenia with anisocytosis

Yoshiyuki Kobayashi,[1,2] Hirotaka Matsui,[1]* Akinori Kanai,[1] Miyuki Tsumura,[2] Satoshi Okada,[2] Mizuka Miki,[2] Kazuhiro Nakamura,[2] Shinji Kunishima,[3] Toshiya Inaba[1] and Masao Kobayashi[2]

[1]Department of Molecular Oncology and Leukaemia Programme Project, Research Institute for Radiation Biology and Medicine, Hiroshima University, [2]Department of Paediatrics, Graduate School of Biomedical and Health Sciences, Hiroshima University, Minami-ku, Hiroshima, and [3]Department of Advanced Diagnosis, Clinical Research Centre, National Hospital Organization Nagoya Medical Centre, Nagoya, Aichi, Japan

Received 29 June 2012; accepted for publication 22 October 2012

Correspondence: Hirotaka Matsui, Department of Molecular Oncology and Leukemia Program Project, Research Institute for Radiation Biology and Medicine, Hiroshima University, 1-2-3 Kasumi, Minami-ku, Hiroshima 734-8553, Japan.
E-mail: hmatsui@hiroshima-u.ac.jp

Summary

αIIbβ3 integrin mutations that result in the complete loss of expression of this molecule on the platelet surface cause Glanzmann thrombasthenia. This is usually autosomal recessive, while other mutations are known to cause dominantly inherited macrothrombocytopenia (although such cases are rare). Here, we report a 4-generation pedigree including 10 individuals affected by dominantly inherited thrombocytopenia with anisocytosis. Six individuals, whose detailed clinical and laboratory data were available, carried a non-synonymous *ITGB3* gene alteration resulting in mutated integrin β3 (ITGB3)-L718P. This mutation causes partial activation of the αIIbβ3 complex, which promotes the generation of abnormal pro-platelet-like protrusions through downregulating RhoA (RHOA) activity in transfected Chinese Hamster Ovary cells. These findings suggest a model whereby the integrin β3-L718P mutation contributes to thrombocytopenia through gain-of-function mechanisms.

Keywords: integrin β3 L718P mutation, familial thrombocytopenia, autosomal dominant inheritance, whole exome sequencing, inhibition of RhoA.

Lifelong haemorrhagic syndromes are in part caused by point mutations in the *ITGA2B* and *ITGB3* genes encoding ITGA2B and ITGB3 proteins (integrin αIIb and β3, respectively). The αIIbβ3 complex regulates thrombopoiesis by megakaryocytes and aggregation of platelets in response to extracellular stimuli, such as ADP and collagen. The autosomal recessive syndrome, Glanzmann thrombasthenia, is the most frequently encountered disease caused by αIIbβ3 mutations (George *et al*, 1990; Nurden, 2006; Nurden & Nurden, 2008; Nurden *et al*, 2011a). Patients have a homozygous or a compound heterozygous mutation in the *ITGA2B* or *ITGB3* genes that causes loss of function of the αIIbβ3 complex. Although platelet counts and size are generally normal, patients typically have severe mucocutaneous bleeding, such as epistaxis, menorrhagia and gastrointestinal bleeding, frequently because of defects in platelet aggregation.

Mutations of the αIIbβ3 complex are also involved in congenital haemorrhagic diseases other than Glanzmann thrombasthenia (Ghevaert *et al*, 2008; Schaffner-Reckinger *et al*, 2009; Jayo *et al*, 2010; Kunishima *et al*, 2011; Nurden *et al*, 2011b). For example, the integrin β3 D723H mutation is found in autosomal dominant macrothrombocytopenia (Ghevaert *et al*, 2008). Biochemical analysis revealed that integrin β3-D723H is a gain of function mutation which activates the αIIbβ3 complex constitutively, albeit only partially. This results in the formation of proplatelet-like protrusions in transfected Chinese Hamster Ovary (CHO) cells, a model of relevance for the formation of macrothrombocytes (Ghevaert *et al*, 2008; Schaffner-Reckinger *et al*, 2009).

More recently, a sporadic patient carrying an integrin β3-L718P mutation was reported (Jayo *et al*, 2010). She had mild thrombocytopenia (127×10^9/l), platelet anisocytosis and reduced platelet aggregation potential. This mutation also induces abnormal proplatelet formation.

In the present study, we report a pedigree with a total 10 of individuals affected by a dominantly inherited haemorrhagic

First published online 17 December 2012
doi:10.1111/bjh.12160

syndrome. Six individuals whose detailed clinical and laboratory data are available, presented with thrombocytopenia accompanied by anisocytosis and carry a non-synonymous *ITGB3* T2231C alteration resulting in the integrin β3-L718P mutation. We also performed entire exon sequencing by a next-generation sequencing and found that the integrin β3-L718P mutation is most likely the sole gene responsible for thrombocytopenia in this pedigree.

Materials and methods

Written informed consent was obtained from individuals in the family in accordance with the Declaration of Helsinki for blood sampling and analysis undertaken with the approval of the Hiroshima University Institutional Review Board.

Patient

The patient was 4-year-old Japanese girl (iv.3 in Fig 1A), who presented with mild bleeding tendencies, such as recurrent nasal bleeding and purpura in her extremities. Her platelet count was 49–72 × 10^9/l with a mean platelet volume (MPV) of 9·8–10·9 fl. White blood cell and red blood cell counts were within the normal range and there were no morphological abnormalities including inclusions in neutrophils. Bone marrow examination was not performed. A total of six of her relatives, namely her father (iii.2), sister and brother (iv.1 and iv.2), two cousins (iv.4 and iv.5) and an aunt (iii.5), were subsequently found to have low platelet counts and were referred to our institute for further investigation.

Antibodies and reagents

Unconjugated or phycoerythrin-cyanin 5 (PC5)-conjugated anti-CD41 monoclonal antibody (Ab) (clone P2) against the αIIbβ3 complex (Beckman Coulter, Brea, CA, USA), fluorescein isothiocyanate (FITC)-conjugated anti-CD41a monoclonal Ab (clone HIP8) (Beckman Coulter), FITC- or peridinin chlorophyll (PerCP)-conjugated anti-CD61 monoclonal Ab (clone RUU-PL 7F12) (BD Biosciences, San Jose, CA, USA), FITC-conjugated PAC-1 (BD Biosciences) and Alexa488-conjugated human fibrinogen (Life Technologies, Carlsbad, CA, USA) were used in flow cytometry. Anti-CD61 monoclonal Ab (clone EP2417Y) (Abcam, Cambridge, UK), anti-DDDDK-tag polyclonal Ab (Medical & Biological Laboratories, Nagoya, Japan), Alexa488-conjugated phalloidin and Hoechst 33342 (both Life Technologies) were used for immunofluorescence microscopy. The oligopeptide Arg-Gly-Asp-Ser (RGDS) (Sigma–Aldrich, St Louis, MO, USA) was used to competitively inhibit the binding of ligands to αIIbβ3, and adenosine diphosphate (ADP) (nacalai tesque, Kyoto, Japan) was used for the stimulation of αIIbβ3 on platelets.

Construction and transfection of expression vectors

Full-length wild type (WT) *ITGA2B* and *ITGB3* cDNA were amplified by polymerase chain reaction (PCR) and cloned into pcDNA3·1 expression vectors. A PCR-mediated site-directed mutagenesis technique was applied to produce *ITGB3* mutants encoding integrin β3-L718P, -D723H and -T562N with or without truncation at the C-terminal side of Y^{759} (del. 759). *RHOA* cDNA, which encodes RhoA (RHOA) protein, was amplified by PCR and its mutants (T19N and Q63L) were generated by site-directed mutagenesis, followed by cloning into p3xFLAG-CMV-10 vectors (Sigma–Aldrich). The *ITGA2B* and *ITGB3* expression vectors were simultaneously transfected into CHO cells cultured in Ham's F12 medium supplemented with 10% fetal bovine serum at 37°C, in 5% CO_2, using Lipofectamine LTX reagent (Life Technologies) according to the manufacturer's instructions.

Immunofluorescent laser-scanning confocal microscopy

Cells grown on coverslips coated with 100 μg/ml fibrinogen were fixed with 4% paraformaldehyde, followed by permeabilization with phosphate-buffered saline containing 0·1% Triton X100. After blocking, the cells were stained with primary antibodies at appropriate dilutions, followed by staining with Alexa488- or Cy3-conjugated secondary antibodies together with Hoechst 33342. High-resolution immunofluorescent images were taken under a laser-scanning confocal microscopy (LSM5 Pascal, Carl Zeiss, Oberkochen, Germany) using a x63 objective.

Flow cytometry

The expression and activation of integrin αIIb and β3 on the platelet surface was indirectly estimated by flow cytometry with the antibodies described above. Mean fluorescence intensity (MFI) of values in an affected individual were divided by those in an unrelated normal control and recorded as relative MFI value (%). For the quantitative determination of αIIbβ3 molecules on the platelet surface, QIFIKIT (Dako, Glostrup, Denmark) was used according to the manufacturer's instructions. MFI of the calibration beads containing five populations (antibody-binding capacity: 2600, 9900, 46 000, 221 000 and 741 000) were 16·12, 63·83, 262·84, 1483·2 and 3772·1, respectively, whereas that of the negative control sample was 1·62. Therefore, αIIbβ3 molecules (copies/platelet) was calculated as $10^{(1.022 \times \log(\mathrm{MFI}) + 2.1679)} - 241$. Activation of platelets and CHO cells was estimated by methods previously described (Shattil *et al*, 1987; Hughes *et al*, 1996). Activation index was defined as $(F-F_0) / (F'-F_0)$, where F is the MFI of PAC-1-stained CHO cells transfected with αIIbβ3-L718P or αIIbβ3-D723H, and F_0 and F' are those transfected with αIIbβ3-WT and αIIbβ3-T562N, respectively. The samples were analyzed on a FACS Calibur (Becton Dickinson, Franklin Lakes, NJ, USA), equipped with an argon laser operating at 488 nm.

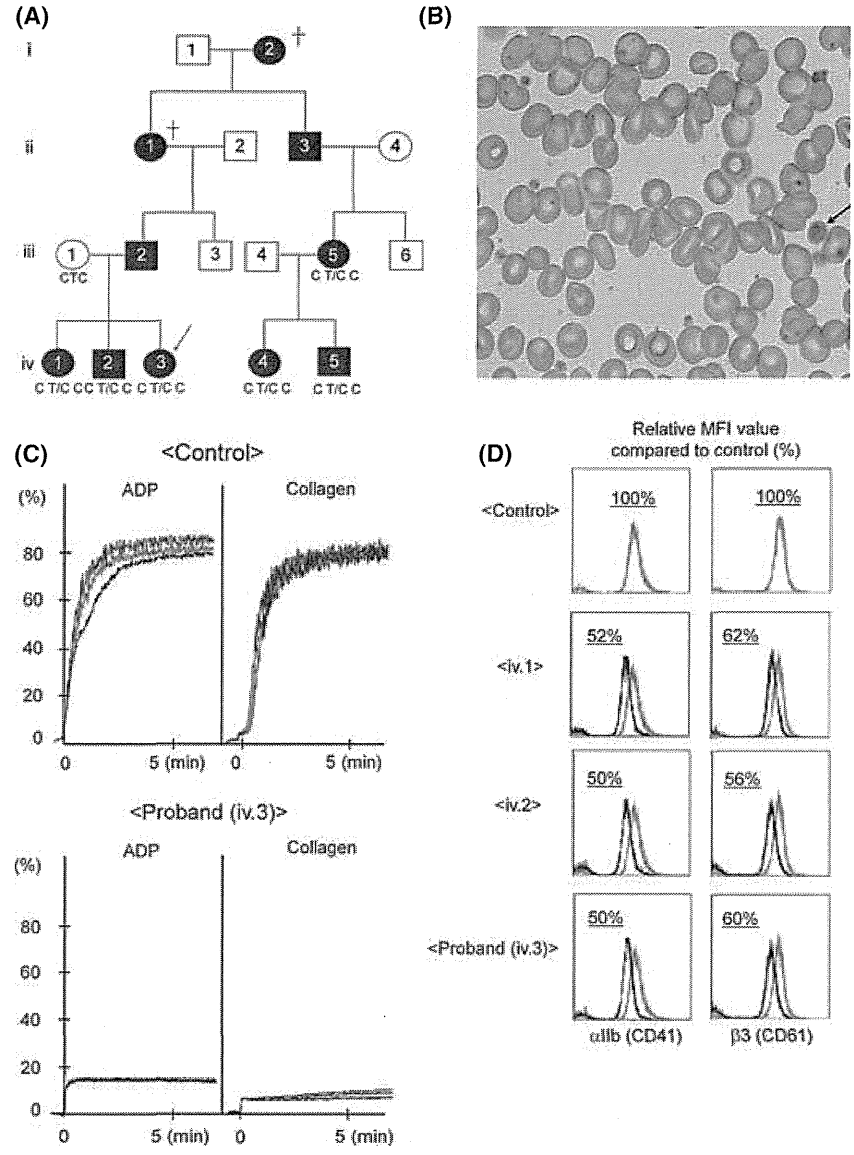

Fig 1. Platelet morphology and aggregation tracings. (A) The pedigree shows affected (filled) and unaffected (open) females (circles) and males (squares). The patient is indicated by an arrow. (B) Platelet morphology as determined by optical microscopy. Peripheral blood specimen obtained from the patient stained with May-Giemsa. The arrow indicates a macrothrombocyte. Original magnification × 600. (C) Representative platelet aggregation tracings in response to ADP and collagen stimuli in platelet-rich plasma from the patient and an unrelated normal control. (D) Flow cytometry of surface integrin αIIb (CD41) and β3 (CD61) expression. Samples were obtained from three affected individuals of the pedigree and an unrelated normal control. Data were calculated as relative MFI value (%), where MFIs of affected individuals were divided by MFI of a control sample.

Exome sequencing

Genomic DNA was obtained from four affected individuals in the pedigree and whole exome sequencing was performed. Briefly, 3 μg genomic DNA was fragmented by Covaris S2 (Covaris, Woburn, MA, USA) and ligated to adaptors, followed by hybridization to biotinylated RNA baits according to the manufacturer's instruction (Agilent Technologies, Santa Clara, CA, USA). The generated sequence tags were sequenced by the 76 bp paired-end protocol of Illumina GAIIx (Illumina, San Diego, CA, USA) and mapped onto the human genomic sequence (hg18, UCSC Genome Browser) using the sequence alignment program Eland (Illumina). Unmapped or redundantly mapped sequences were removed from the data set, and only uniquely mapped sequences were used for further analyses. Positions relative to RefSeq genes were calculated based on the respective genomic coordinates. Genomic coordinates of exons and the protein-coding regions of the RefSeq transcripts are as described in hg18. To verify the presence of *ITGB3* gene alteration, amplification and direct sequencing of a part of exon 14 was performed with the following primers; 5′-CATAGCCAGTTCAAGTGACTCCTG-3′ for forward primer and 5′-ACGATGGTACTGGCTGAACATGAC-3′ for reverse primer.

Results

Pedigree of a family with autosomal dominant thrombocytopenia with anisocytosis

In the original patient, marked platelet anisocytosis was observed in peripheral blood samples (Fig 1B). Platelet aggregation induced by ADP (1–4 μmol/l) and collagen (0·5–2 μg/ml) was markedly reduced (Fig. 1C and Table I), but agglutination induced by ristocetin (1·25 mg/ml) was within

the normal range (data not shown). Three affected individuals (iii.5, iv.1, and iv.2) showed abnormalities in platelet function similar to those of the original patient. In these affected individuals, the αIIb and β3 expression levels, which were indirectly estimated as relative MFI value (%), were 43–75% of a healthy control (Fig 1D and Table I). The number of αIIbβ3 molecules on the platelet surface in patients, as evaluated by flow cytometry using QIFIKIT, was 35 000–38 400 copies/platelet (MFI: 212·1 –232·4), whereas in an unaffected individual of the pedigree (iii.1) and an unrelated control, there were 65 200 and 62 100 copies/platelet (MFI: 389·2 and 371·3), respectively (Table I). The tendency to bleed was mild to moderate, as exemplified by the following episodes: when family member iv.1 received a bruise to the face, treatment with recombinant Factor VIIa was required because of persistent epistaxis; also, family member iii.5 had had to give birth by Caesarean section because of low platelet count. The family pedigree (Fig 1A), which shows no evidence of consanguineous marriage, strongly suggests the inheritance of thrombocytopenia as an autosomal dominant trait. The laboratory findings are shown in Table I.

Identification of the integrin β3 L718P mutation by whole exome analysis

To isolate a candidate gene alteration responsible for the thrombocytopenia, whole exome sequencing analysis was performed using genomic DNA obtained from the patient (iv.3), her sister and brother (iv.1 and iv.2) and a cousin (iv.4). A total of 794 non-synonymous gene alterations among 1551 SNPs that are not registered in dbSNP 129/130 were detected in the patient. To isolate the responsible gene, we selected non-synonymous gene alterations shared by the four affected individuals as strong candidates. Among the 90 alterations commonly found in the affected individuals of the pedigree (individual numbers of SNPs/mutations are shown in Table II), we focused on the heterozygous non-synonymous T2231C alteration in exon 14 of the *ITGB3* gene, which results in the substitution of leucine at 718 for proline (L718P) in the integrin β3 protein. We selected this because it was recently reported as a candidate mutation responsible for thrombocytopenia (Jayo *et al*, 2010). The presence of the mutation in six affected individuals of the pedigree (iv.1, iv.2, iv.3, iv.4, iii.5 and iv.5) and its absence in an unaffected individual (iii.1) and an unrelated control was confirmed by a direct-sequencing (Fig 2). As far as we could determine, no other non-synonymous gene alterations previously reported to cause thrombocytopenia or defective platelet function were present in the affected individuals of the pedigree. In addition, the L718 residue in integrin β3 is well-conserved between species and amino acid substitution in this position is predicted by bioinformatic tools, including Polyphen and SIFT, to cause a significant change in protein structure and function (data not shown). These observations strongly suggest that the L718P mutation in integrin β3 is the responsible gene alteration that causes familial thrombocytopenia.

Constitutive but partial activation of the αIIbβ3 complex by β3-L718P

To elucidate the effects of the integrin β3-L718P mutation on the activation status of αIIbβ3 complexes in resting or ADP-activated platelets, fresh platelets were analysed by flow cytometry using PAC-1, a ligand-mimicking antibody that specifically recognizes the activated form of the αIIbβ3 complex (Shattil *et al*, 1987).

Resting control platelets from healthy individuals bound PAC-1 with a similar affinity to those treated with RGDS, a peptide which competitively inhibits the binding of ligands for

Table I. Laboratory data of seven individuals of the pedigree.

						Relative MFI value compared to control (%)		αIIbβ3	molecules	Platelet (%)	aggregation
Patient	Sex	Age (years)	Platelet count ($\times 10^9$/l)	MPV (fl)	PDW (%)	αIIb	β3	MFI	copies/platelet	ADP (4 μM)	collagen (2·0 μg/ml)
iii.1	F	37	210	10·2	12·1	110	111	389·2	65 200	NA	NA
iii.5	F	34	38–67	8·5–11·3	10·0–19·0	43	75	NA	NA	15	12
iv.1	F	11	30–43	7·8–11·2	9·7–16·3	52	62	232·4	38 400	16	8
iv.2	M	8	49–64	10·3–11·1	10·1–14·7	50	56	216·4	35 700	23	16
iv.3	F	6	49–72	9·8–10·9	11·1–13·3	50	60	212·1	35 000	12	8
iv.4	F	4	32–59	9·9–10·8	12·3–15·6	NA	NA	NA	NA	NA	NA
iv.5	M	2	28–50	8·9–9·0	18·0–18·4	49	51	NA	NA	NA	NA

MPV, mean platelet volume (normal range: 9·4–12·3 fl); PDW, platelet distribution width (normal range: 9·5–14·8 %); NA, not available.
αIIbβ3 molecules (copies/platelet) were calculated as $10^{(1.022 \times \log(\mathrm{MFI}) + 2.1679)} - 241$ (see *Materials and methods*).

Table II. Number of SNPs/mutations detected by whole exome sequencing.

Case	iv.1	iv.2	iv.3	iv.4
SNP	21 531	21 697	20 413	20 113
Not in dbSNP	1 674	1 722	1 473	1 551
129 and 130				
Non-synonymous alternations				
Homozygous	62	58	65	42
Heterozygous	800	815	667	752
Non-synonymous (common)	90			

αIIbβ3 complex such as fibrinogen and PAC-1 (Fig 3A, compare black and blue lines), indicating that wild-type αIIbβ3 in resting platelets is not activated. In contrast, platelets obtained from the affected individuals (iii.5, iv.1, iv.2 and iv.3) showed a slight increase of PAC-1 binding compared to those treated with RGDS (Fig 3A). Indeed, resting platelets from affected individuals showed a slight but significant increase of PAC-1 binding relative to healthy individuals (Fig 3A, top panel). In addition, flow cytometric analysis using FITC-conjugated fibrinogen also showed a significant increase of fibrinogen binding potential in resting platelets from affected individuals compared with healthy controls (bottom panel). Because MPV (shown in Table I) did not exceed the normal range (9·4–12·3 fl) and surface expression levels of αIIbβ3 were lower in patients than controls (Fig 1D), it is proposed that these observations indicate spontaneous activation of αIIbβ3-L718P in resting platelets.

ADP-activated platelets from healthy volunteers, on the other hand, bound to PAC-1 with a very high affinity (Fig 3B, red lines and 3B, top panel), as expected. In contrast, only a small increase of affinity to PAC-1 was observed in ADP-treated platelets carrying the β3-L718P mutation, resulting in a marginal increase of binding potential (bottom panel). These findings suggest that αIIbβ3-L718P is partially activated in the absence of inside-out signals such as ADP, but nevertheless cannot be fully activated in the presence of such signals.

To confirm the contribution of the integrin β3-L718P mutation to spontaneous activation of αIIbβ3, CHO cells were transiently transfected with expression vectors encoding integrin β3-WT, -L718P, -D723H or -T562N together with a vector encoding αIIb-WT. Flow cytometric analysis (Fig 3C) revealed that αIIbβ3-L718P expressed in CHO cells bound to PAC-1 to the same degree as αIIbβ3-D723H, a mutant previously reported to partially activate αIIbβ3, and to a lesser extent than a fully active αIIbβ3-T562N mutant (Kashiwagi *et al*, 1999). We calculated the activation indices (see *Materials and methods*) (Hughes *et al*, 1996; Schaffner-Reckinger *et al*, 2009) of αIIbβ3-L718P and -D723H as 0·23 ± 0·07 and 0·16 ± 0·02, respectively, taking αIIbβ3-T562N as fully active (=1·0) and αIIbβ3-WT as inactive (=0) (Fig 3D). Because CHO cells were not stimulated by ADP in this experiment, each index represents αIIbβ3 activation status at rest.

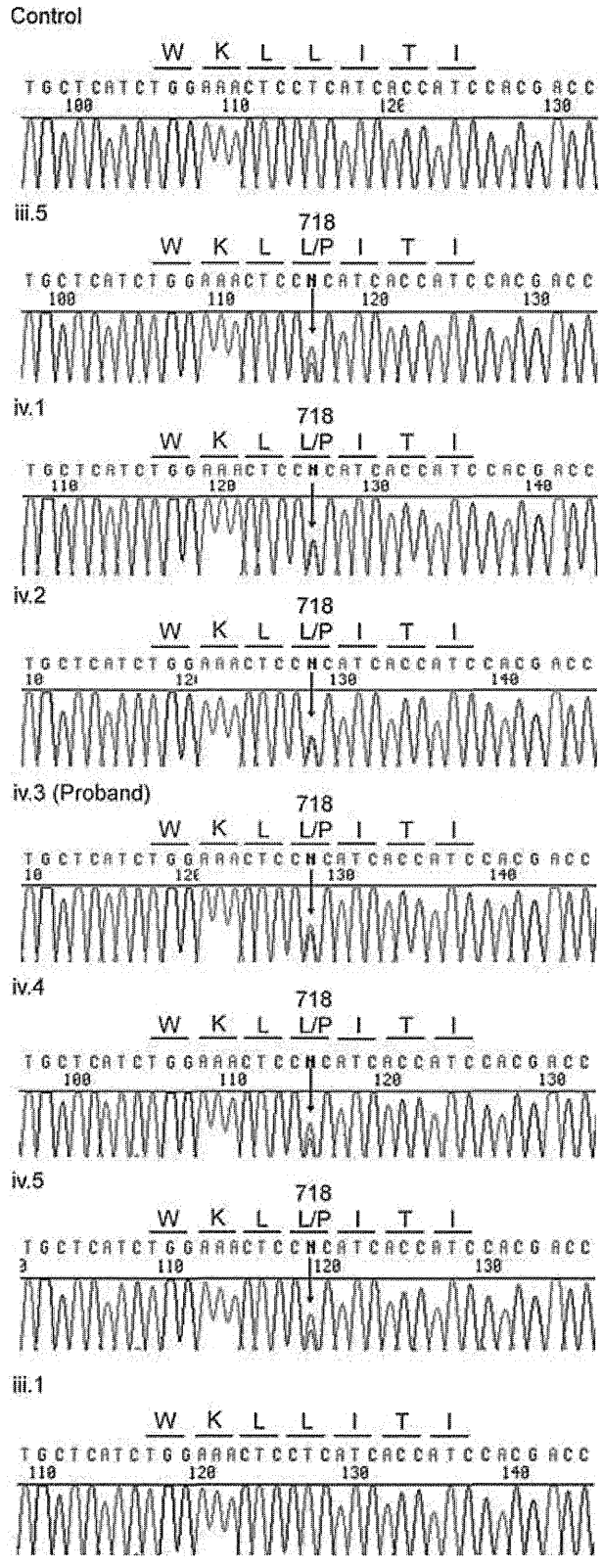

Fig 2. Direct sequencing analysis around T2231 in exon 14 of the *ITGB3* gene. Genomic DNA extracted from the affected and unaffected individuals of the pedigree were amplified by polymerase chain reaction and sequenced. Arrows indicate the position of the T2231 mutation in the *ITGB3* gene.